A unified variational approach for coupling 3D–1D models and its blood flow applications

P.J. Blanco [a,*], R.A. Feijóo [a] and S.A. Urquiza [b]

[a] *LNCC, Laboratório Nacional de Computação Científica, Av. Getúlio Vargas 333, Quitandinha, 25651–075, Petrópolis, RJ, Brazil, e–mail: pjblanco@lncc.br, feij@lncc.br*

[b] *Laboratorio de Bioingeniería, Universidad Nacional de Mar del Plata, Av. J.B. Justo 4302, 7600 Mar del Plata, Argentina, e–mail: santiagourquiza@fi.mdp.edu.ar*

Abstract

In this work, we propose an extended variational formulation in order to handle the problem of the flow of an incompressible fluid in compliant vessels with discontinuous fields. This approach makes possible to tackle in a consistent variational manner problems like the coupling between models of different dimensionality. The main ideas of the work are presented for a simple heat transfer problem and then are used in the context of modelling blood flow in large vessels. A computational implementation of the proposed formulation is also shown and discussed by presenting examples of practical applications.

Key words: Variational formulation, discontinuous fields, coupling conditions, multidimensional models, hemodynamics.

1 Introduction

Computational modelling provides a powerful tool to study and correlate the onset and progress of some cardiovascular diseases with the local patterns of the blood flow [6,13,23,35]. Accordingly, the detailed modelling of fluid mechanics processes on some specific arterial districts has become increasingly important to understand the local hemodynamic phenomena [26,30].

* Corresponding author.
Email address: pjblanco@lncc.br (P.J. Blanco).

Modelling the fluid mechanics aspects of blood flow involves several challenging issues that must be accounted for in order to achieve ever–increasing levels of realism in computational simulations. Among others, one of the most relevant aspects of the problem is the fluid–structure interaction derived from the coupling between the compliant properties of the vessel walls and the blood flow. This feature defines the propagatory nature of the pulse wave which, in turn, poses the problem of setting appropriate boundary conditions when a particular district is artificially isolated from the rest of the network. It is possible to mention at least three ways of tackling this subject: the classical one is based on obtaining boundary conditions by estimations or measurements (see for instance [28,29]). The second one, presented recently in [39], is based on computing what was called a Dirichlet–to–Neumann mapping that takes into account the phenomena occurring downstream the 3D region through the computation of the downstream vascular impedance. However, this method is actually derived only for outflow boundary conditions and also under time–periodic assumptions, which may result too restrictive to accommodate the complex situations encountered in practice. Finally, the third possibility is based on the use of coupled 3D–1D models where some zones are modelled at a high level of detail (3D domain) while the remaining part of the system is simplified to a 1D formulation. In this way, it is possible to achieve in a natural manner the systemic response of the whole arterial tree. Investigations in this direction were pioneered in [10] and continued afterwards in [11,12,37]. Lastly, the coupling between 3D and 0D models (see for instance [24,36]) could be interpreted in the same way as the third possibility, that is in the context of multidimensional models.

While the second approach is by far more suitable than the classical one, is the later the more appropriate in order to consider all the complex interactions that occur within the whole system operating as a fully integrated functional ensemble. This assertion must be understood regarding the capability of automatically adapting boundary conditions to what happens beyond the limits of the 3D domain, either in time–varying conditions or during parameter adjustment in the context of sensitivity analysis.

Several authors [10,11,37] have treated the problem of coupling full 3D models based on the Navier Stokes equations in compliant domains with reduced 1D models by making a priori assumptions directly incorporated into the partial differential equation problem. This is done by prescribing the continuity of some of the involved quantities (for instance flow rate and mean pressure) at the coupling interfaces. Nevertheless, it must be noted that discontinuities may emerge from the use of incompatible models at both sides of a given coupling interface because of differences in the underlying kinematics, as well as from the use of different levels of approximation for each part of the original domain. For instance, in ref. [37], the continuity of the pressure (actually the normal traction) between 3D and 1D models is stated in a weak sense. This, in turn,

implies, in a point–wise sense, the existence of a possible jump in the pressure field when dealing with the corresponding discrete problem. Moreover, when using elastic models for the arterial wall the area is uniquely determined by the value of the internal pressure. As a consequence, the area of the vessel at both sides of the coupling interfaces may differ from each other. This issue was treated in [37] by relaxing the continuity of the cross sectional area, in contrast to that suggested in [11] where this condition was stated as one of the coupling requirements. Consequently, the former alternative conducts to efficient fully coupled schemes where numerical instabilities are practically avoided in contrast to that reported by Formaggia et al., [11]. Despite that, several other sources of discontinuities may be noticed from the non–matching kinematics over the coupling interfaces. For example, the abrupt change on the shape of the velocity profile across an artificial internal boundary carries out relative jumps on the linear momentum and wall shear stress. Observe that such a change in the velocity profile can be interpreted as being consequence of a selection of somehow incompatible kinematical reduction hypothesis over the 1D portion of the model. Conversely, in ref. [12,15] the coupling of multidimensional models is understood as a problem with a priori defective boundary conditions on the 3D model due to the mismatch between the information available at both sides of the interfaces. In fact, in those works the theory for 3D models with boundary conditions based upon mean quantities is developed. Within this approach the problem is interpreted as ill–posed since one has full 3D fields at one side of the interface and only mean quantities at the other side. Consequently, some supplementary assumptions are introduced in order to "close" the problem.

Alternatively, the present work aims at tackling this situation from a different perspective. Observe that a ND ($N = 0, 1, 2$) simplified model can be viewed as a reduction of a complete 3D model by means of kinematical restrictions introduced on a part of a given domain. Performing such kinematical assumptions allows us to reduce the full problem over that part of the domain to a 2D, a 1D or even a 0D lumped problem. By looking at the whole domain again we realize that, due to the dissimilarity between the underlying kinematics, we generated discontinuities in the involved fields. Therefore, the original variational formulation, valid for fields that are continuous in the sense of the trace of the functions over such a coupling interface, makes no sense in this new situation. For this reason it is necessary to reformulate the problem, rewriting the variational principle in order to accommodate those discontinuities. Hence, the main goal of the present work is to formulate an extended variational principle for problems where fields can become discontinuous at some artificial internal boundary, that will be regarded as the coupling interface. Moreover, we recast this problem within a unified variational statement from which the coupling conditions are naturally derived. The conception of such a consistent unified variational formulation of the coupled problem is very desirable when performing, for instance, stability and error analysis on the

corresponding numerical schemes.

Although the application of these ideas to hemodynamic modelling is of our main concern, this issue is inherent to a great variety of problems, and other examples can easily be devised. For instance, the fluid–structure interaction problem may involve different interpolations for the fluid and the solid domain, as well as joining 3D solid models with shell models or even beam components may lead to discontinuous fields.

This work is organized as follows, in Section 2 a simple example is conducted so as to outline the ideas behind this approach, formulating the coupling between models of different dimensionality for the heat transfer problem. In Section 3 we address a classical statement for the problem of the flow of an incompressible fluid in a compliant vessel, whilst in Section 4 this problem is extended within the theoretical context of discontinuous fields. In Section 5 an approximation of the problem presented in Section 4 is performed and a discrete counterpart is given. Finally, in Section 6 several numerical experiments are presented illustrating the capabilities of this approach in cardiovascular modelling. In addition, situations where spurious reflections arise are identified.

2 Extended variational formulation for the heat transfer problem

In this section we present a simple example where the main idea of extending a variational statement is introduced. Let $\Omega \subset \mathbb{R}^{n_d}$ $(n_d = 2, 3)$ with boundary Γ and consider the variational formulation for the heat transfer problem: *find* $\theta \in \mathcal{X}$ *such that*

$$\int_\Omega k \nabla\theta \cdot \nabla\eta \, \mathrm{d}\mathbf{x} = \int_\Omega f\eta \, \mathrm{d}\mathbf{x} \qquad \forall \eta \in \mathcal{Y}, \tag{1}$$

where k is the conductivity coefficient assumed to be constant for the sake of simplicity and f is a volume source. Regularity and essential boundary conditions are accounted by the set $\mathcal{X} = \mathcal{Y} + \bar{\theta}$, being $\mathcal{Y} = \{\theta \in H^1(\Omega);\, \theta = 0 \text{ on } \Gamma_D\}$, and $\bar{\theta}$ is an arbitrary element of $\mathcal{X}$ satisfying the Dirichlet boundary condition prescribed on Γ_D. Without loss of generality we consider that $\Gamma_D = \Gamma$.

Let Γ_c be an artificial internal boundary that allows us to make a partition of domain Ω, according to Figure 1 (here a 2D domain for simplicity), into subdomains Ω_1 and Ω_2 with boundaries Γ_1 and Γ_2 respectively. Thus we have $\Omega = \Omega_1 \cup \Omega_2 \cup \Gamma_c$, $\Gamma_c = \Gamma_1 \cap \Gamma_2$ and $\Gamma = (\Gamma_1 \cup \Gamma_2) \setminus \Gamma_c$.

As a consequence of the regularity of functions in $\mathcal{X}$ we have that the traces

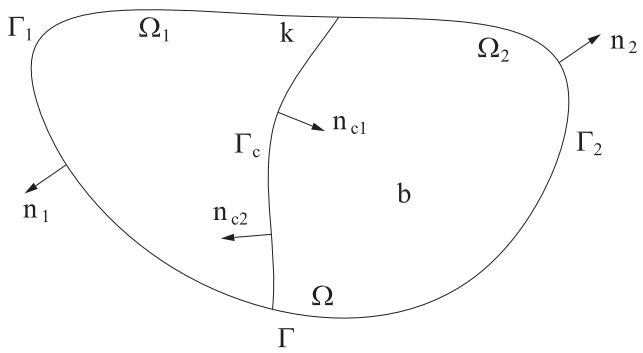

Fig. 1. Split of domain Ω.

of θ_1 and θ_2 coincide over boundary Γ_c, and we must also consider that $\theta = \bar{\theta}$ on Γ_D. Hence, the Euler–Lagrange equations associated to the variational problem (1), regarding the splitting of the domain Ω, are given by

$$\begin{cases} -k\triangle\theta_1 = f & \text{in } \Omega_1, \\ -k\triangle\theta_2 = f & \text{in } \Omega_2, \\ k\nabla\theta_1 \cdot \mathbf{n}_{c1} = k\nabla\theta_2 \cdot \mathbf{n}_{c1} & \text{on } \Gamma_c, \end{cases} \tag{2}$$

where $\mathbf{n}_{c1}$ is the unit normal vector of boundary Γ_c (from domain Ω_1). In obtaining this set of equations it has been used the fact that $\theta_1 = \theta_2$ on Γ_c, that is a consequence of the regularity of the functions in the space $\mathcal{Y}$.

For some reason that will be clarified later, we would like to enlarge the admissible function set $\mathcal{X}$, allowing functions to be discontinuous at Γ_c. In this context, it is clear that the variational formulation (1) makes no sense and must be altered in order to ensure that the solution of this extended problem responds to the same Euler equations that those of the original problem. The idea behind this modified variational formulation is to incorporate additional terms based on the virtual power performed by the discontinuities of the unknowns on the interface. More precisely, let $\mathcal{X}_d = \mathcal{X}_1 \times \mathcal{X}_2$ where $\mathcal{X}_1 = \{\theta_1 \in H^1(\Omega_1);\ \theta_1 = \bar{\theta}_{|\Gamma_{1D}} \text{ on } \Gamma_{1D}\}$ and $\mathcal{X}_2 = \{\theta_2 \in H^1(\Omega_2);\ \theta_2 = \bar{\theta}_{|\Gamma_{2D}} \text{ on } \Gamma_{2D}\}$. Observe that $\mathcal{X}_d$ is a larger set, i.e., $\mathcal{X} \subset \mathcal{X}_d$. We also introduce variables $r_1 \in \mathcal{Z}_1, r_2 \in \mathcal{Z}_2$, being $\mathcal{Z}_1$ and $\mathcal{Z}_2$ proper function sets. In this particular case $\mathcal{Z}_1 = \mathcal{Z}_2 = H^{-1/2}(\Gamma_c)$. Index i will correspond to part Ω_i, $i = 1, 2$. Then, there exists a γ–family of equivalent variational formulations for the extended problem that reads as follows: *for some* $\gamma \in [0, 1]$, *find* $(\theta, r_1, r_2) \in \mathcal{X}_d \times \mathcal{Z}_1 \times \mathcal{Z}_2$

such that

$$\begin{aligned}\int_{\Omega_1} k\nabla\theta_1\cdot\nabla\eta_1\ \mathrm{d}\mathbf{x} + \int_{\Omega_2} k\nabla\theta_2\cdot\nabla\eta_2\ \mathrm{d}\mathbf{x}& \\ +\gamma\int_{\Gamma_c} r_1(\eta_1-\eta_2)\ \mathrm{d}\Gamma + (1-\gamma)\int_{\Gamma_c} r_2(\eta_1-\eta_2)\ \mathrm{d}\Gamma& \\ +\gamma\int_{\Gamma_c} s_1(\theta_1-\theta_2)\ \mathrm{d}\Gamma + (1-\gamma)\int_{\Gamma_c} s_2(\theta_1-\theta_2)\ \mathrm{d}\Gamma& \\ =\int_{\Omega_1} f\eta_1\ \mathrm{d}\mathbf{x} + \int_{\Omega_2} f\eta_2\ \mathrm{d}\mathbf{x} \qquad \forall(\eta,s_1,s_2)\in\mathcal{Y}_d\times\mathcal{Z}_1\times\mathcal{Z}_2,& \quad (3)\end{aligned}$$

with $\eta=(\eta_1,\eta_2)\in\mathcal{Y}_d$ the admissible variations of functions in $\mathcal{X}_d$ given by

$$\begin{aligned}&\mathcal{Y}_d=\mathcal{Y}_1\times\mathcal{Y}_2,\\ &\mathcal{Y}_1=\{\eta_1\in H^1(\Omega_1);\ \eta_1=0 \text{ on } \Gamma_{1D}\},\\ &\mathcal{Y}_2=\{\eta_2\in H^1(\Omega_2);\ \eta_2=0 \text{ on } \Gamma_{2D}\}.\end{aligned} \quad (4)$$

It is readily verified that the Euler–Lagrange equations associated to the family of variational formulations (3), just in terms of θ, are the following

$$\begin{cases}-k\triangle\theta_1=f & \text{in } \Omega_1,\\ -k\triangle\theta_2=f & \text{in } \Omega_2,\\ k\nabla\theta_1\cdot\mathbf{n}_{c1}=k\nabla\theta_2\cdot\mathbf{n}_{c1} & \text{on } \Gamma_c,\\ \theta_1=\theta_2 & \text{on } \Gamma_c,\end{cases} \quad (5)$$

where $r_\gamma=\gamma r_1+(1-\gamma)r_2=-k\nabla\theta_1\cdot\mathbf{n}_{c1}=-k\nabla\theta_2\cdot\mathbf{n}_{c1}$. Observe that the solution of the variational problem (3) satisfies the same Euler equations than the variational problem (1). In this way it is possible, from a variational context, to recover information of the original problem without imposing conditions or restrictions over function sets $\mathcal{X}_1$ and $\mathcal{X}_2$ at Γ_c. The advantage here is the arbitrariness in choosing sets $\mathcal{X}_1$ and $\mathcal{X}_2$.

Remark 1 *On one hand, problem* (3) *resembles those variational formulations derived from domain decomposition techniques [5]. Indeed, the present approach may be regarded as a generalization, since by taking* $r_\gamma=\gamma r_1+(1-\gamma)r_2$ *as a unique variable within the problem we recover those methods. On the other hand, by taking* $\gamma=\frac{1}{2}$ *we recover another class of formulations arising when minimizing relaxed functionals [9].*

Remark 2 *Notice that, for any associated discrete problem, formulation* (3) *allows us to consider non–matching meshes for domains* Ω_i, $i=1,2$ *at both sides of the internal boundary* Γ_c. *In this case* r_1 *and* r_2 *may pertain to different finite–dimensional spaces. Therefore, for each value of* γ, *the sense in which the Euler equations are satisfied is strongly related to the characteristics of each mesh.*

In anticipation of treating the coupling problem between hemodynamics models of different dimensionality, we will present at this stage the simple case of coupling 3D–1D models for the heat transfer equations. This situation can be thought of as a problem where discontinuous fields arise due to the difference in the *kinematics* assumed for different parts of the domain.

Let us consider the particular situation exposed in Figure 2 for which we have $\Gamma = \Gamma_A \cup \Gamma_{L_1} \cup \Gamma_{L_2} \cup \Gamma_B$, with essential boundary conditions over Γ_A and Γ_B, namely $\bar{\theta}_A$ and $\bar{\theta}_B$, and with homogeneous Neumann boundary condition over $\Gamma_{L_1} \cup \Gamma_{L_2}$.

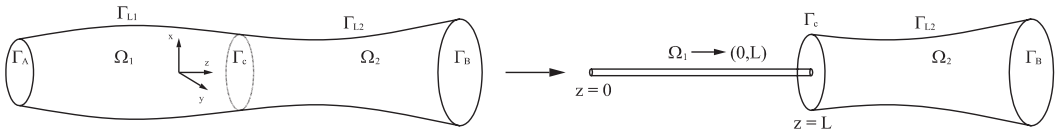

Fig. 2. Coupling 3D–1D models for the heat transfer problem.

In the extended variational formulation (3) we assume the temperature θ_1 to be constant along each transversal section with respect to the axial direction $\mathbf{e}_z$. That is, $\theta_{|\Omega_1} = \theta_1(z)$ where z is the coordinate over $\mathbf{e}_z$ axis. Consequently we denote with $\eta_1(z)$ the admissible variations of the temperature in Ω_1. We also consider r_1 constant on Γ_c. With these assumptions it is possible to integrate along the transversal section and to write a reduced 1D model achieving the following problem: *for some* $\gamma \in [0,1]$, *find* $(\theta_1, \theta_2, r_1, r_2) \in \mathcal{X}_d \times \mathcal{Z}_1 \times \mathcal{Z}_2$ *such that*

$$\begin{aligned}
\int_0^L A(z) k \frac{\partial \theta_1}{\partial z} \frac{\partial \eta_1}{\partial z} \, \mathrm{d}z + \int_{\Omega_2} k \nabla \theta_2 \cdot \nabla \eta_2 \, \mathrm{d}\mathbf{x} \\
+ \gamma \int_{\Gamma_c} r_1(\eta_1 - \eta_2) \, \mathrm{d}\Gamma + (1-\gamma) \int_{\Gamma_c} r_2(\eta_1 - \eta_2) \, \mathrm{d}\Gamma \\
+ \gamma \int_{\Gamma_c} s_1(\theta_1 - \theta_2) \, \mathrm{d}\Gamma + (1-\gamma) \int_{\Gamma_c} s_2(\theta_1 - \theta_2) \, \mathrm{d}\Gamma \\
= \int_0^L \bar{f} \eta_1 \, \mathrm{d}z + \int_{\Omega_2} f \eta_2 \, \mathrm{d}\mathbf{x} \qquad \forall (\eta_1, \eta_2, s_1, s_2) \in \mathcal{Y}_d \times \mathcal{Z}_1 \times \mathcal{Z}_2, \quad (6)
\end{aligned}$$

where $\bar{f} = \int_{\Gamma_z} f \, \mathrm{d}\Gamma$ over each transversal section. In this particular case it is easy to see that, being $\mathcal{X}_d = \mathcal{X}_1 \times \mathcal{X}_2$, we have

$$\begin{aligned}
\mathcal{X}_1 &= \{\theta_1 \in H^1(0,L);\ \theta_1 = \bar{\theta}_A \text{ in } z = 0\}, \\
\mathcal{X}_2 &= \{\theta_2 \in H^1(\Omega_2);\ \theta_2 = \bar{\theta}_B \text{ on } \Gamma_B\}, \\
\mathcal{Z}_1 &= \mathbb{R}, \\
\mathcal{Z}_2 &= H^{-1/2}(\Gamma_c).
\end{aligned} \quad (7)$$

In the following we give the main steps in proving the existence and uniqueness of the solution. Firstly, the existence and uniqueness of the solution $\theta = (\theta_1, \theta_2)$ is straightforwardly proved by using the theory of elliptic problems [5,8,14], for which we have to work with the kernel of the operator $\mathcal{B}$ (associated to

the bilinear form $b(\cdot,\cdot)$ corresponding to the equation of $r_\gamma = \gamma r_1 + (1-\gamma)r_2)$, that is a subspace of $\mathcal{X}_d$. Indeed, let $\mathcal{W}_d = H^1(0,L)\times H^1(\Omega_2)$ equipped with the norm $\|\theta\|_{\mathcal{W}_d} = \|\theta_1\|_{H^1(0,L)} + \|\theta_2\|_{H^1(\Omega_2)}$ and consider the following decomposition $\theta = \mu + \xi$ where $\xi \in \mathcal{W}_d$ is such that $\xi_1(0) = \bar{\theta}_A$, $\xi_1(L) = 0$ and $\xi_{2|\Gamma_B} = \bar{\theta}_B$, $\xi_{2|\Gamma_A} = 0$, while $\mu \in \mathcal{K}_\gamma \subset \mathrm{Ker}(\mathcal{B})$ being

$$\mathcal{K}_\gamma = \Big\{\mu = (\mu_1,\mu_2) \in \mathcal{W}_d; \mu_1(0) = 0,\ \mu_{2|\Gamma_B} = 0,$$
$$\gamma\left[\mu_1(L) - \frac{1}{A_c}\int_{\Gamma_c}\mu_2\ \mathrm{d}\Gamma\right] = 0,\ (1-\gamma)[\mu_1(L) - \mu_{2|\Gamma_c}] = 0\Big\}. \quad (8)$$

Consider the bilinear form $a : \mathcal{K}_\gamma \times \mathcal{K}_\gamma \to \mathbb{R}$

$$a(\mu,\eta) = \int_0^L Ak\frac{\partial\mu_1}{\partial z}\frac{\partial\eta_1}{\partial z}\ \mathrm{d}z + \int_{\Omega_2} k\nabla\mu_2\cdot\nabla\eta_2\ \mathrm{d}\mathbf{x}, \quad (9)$$

that is trivially symmetric, continuous and coercive in $\mathcal{K}_\gamma \times \mathcal{K}_\gamma$ provided $A \in L^\infty(0,L)$ and $A \geq A_o > 0$, $k \geq k_o > 0$ in $(0,L)$ (that is always satisfied). Consider the linear functional $l : \mathcal{K}_\gamma \to \mathbb{R}$ given by

$$l(\eta) = \int_0^L \bar{f}\eta_1\ \mathrm{d}z + \int_{\Omega_2} f\eta_2\ \mathrm{d}\mathbf{x}, \quad (10)$$

that is obviously continuous in $\mathcal{K}_\gamma$ provided $\bar{f} \in H^{-1}(0,L)$ and $f \in H^{-1}(\Omega_2)$. Then, by the Lax–Milgram theorem there exists a unique solution $\mu \in \mathcal{K}_\gamma \subset \mathrm{Ker}(\mathcal{B})$ such that

$$a(\mu,\eta) = \tilde{l}(\eta) \qquad \forall\eta \in \mathcal{K}_\gamma, \quad (11)$$

where $\tilde{l}(\eta) = l(\eta) - a(\xi,\eta)$. Therefore, the existence and uniqueness of $\theta = (\theta_1,\theta_2)$, solution of problem (19) follow. To prove the existence and uniqueness of $r_\gamma \in H^{-1/2}_{[\![\cdot]\!]}(\Gamma_c)$, we need to resort to the theory of mixed problems [5,8,14]. Firstly, let us introduce the following space

$$H^{1/2}_{[\![\cdot]\!]}(\Gamma_c) = \{[\![\mu]\!] \in H^{1/2}(\Gamma_c);\ \mu \in \mathcal{W}_d;\ [\![\mu]\!] = \mu_1(L) - \mu_{2|\Gamma_c}\}, \quad (12)$$

equipped with the norm

$$\|[\![\mu]\!]\|_{H^{1/2}_{[\![\cdot]\!]}(\Gamma_c)} = \inf_{\substack{\varphi\in\mathcal{W}_d \\ [\![\mu]\!]=\varphi_1(L)-\varphi_{2|\Gamma_c}}} \|\varphi\|_{\mathcal{W}_d}. \quad (13)$$

In this case we have a classical mixed problem with a bilinear form $b : \mathcal{Y}_d \times H^{-1/2}_{[\![\cdot]\!]}(\Gamma_c) \to \mathbb{R}$ given by

$$b(\mu, r_\gamma) = \int_{\Gamma_c} r_\gamma(\mu_1 - \mu_2)\ \mathrm{d}\Gamma. \quad (14)$$

Since the bilinear form $b(\cdot,\cdot)$ satisfies the corresponding inf–sup condition, i.e. the existence of $\beta_0 > 0$ such that

$$\beta_0 \leq \inf_{\substack{r_\gamma \in H^{-1/2}_{[\![\cdot]\!]}(\Gamma_c) \\ r_\gamma \neq 0}} \sup_{\substack{\psi \in \mathcal{W}_d \\ [\![\mu]\!] = \psi_1(L) - \psi_{2|\Gamma_c} \\ \psi_1(L) \neq \psi_{2|\Gamma_c}}} \frac{\displaystyle\int_{\Gamma_c} r_\gamma [\![\mu]\!] \, \mathrm{d}\Gamma}{\|\psi\|_{\mathcal{W}_d} \|r_\gamma\|_{H^{-1/2}_{[\![\cdot]\!]}(\Gamma_c)}}, \tag{15}$$

then there exists a unique $r_\gamma \in H^{-1/2}_{[\![\cdot]\!]}(\Gamma_c)$ solution of problem (6). It remains to see (15). Observe that $H^{-1/2}_{[\![\cdot]\!]}(\Gamma_c)$, endowed with the norm

$$\|r_\gamma\|_{H^{-1/2}_{[\![\cdot]\!]}(\Gamma_c)} = \sup_{\substack{[\![\mu]\!] \in H^{1/2}_{[\![\cdot]\!]}(\Gamma_c) \\ [\![\mu]\!] \neq 0}} \frac{\displaystyle\int_{\Gamma_c} r_\gamma [\![\mu]\!] \, \mathrm{d}\Gamma}{\|[\![\mu]\!]\|_{H^{1/2}_{[\![\cdot]\!]}(\Gamma_c)}}, \tag{16}$$

is the dual space of $H^{1/2}_{[\![\cdot]\!]}(\Gamma_c)$ defined in (12). Thus, for any $\beta_1 > 1$ we can choose ψ such that $\psi_1(L) - \psi_{2|\Gamma_c} = [\![\mu]\!]$ and

$$\|\psi\|_{\mathcal{W}_d} \leq \beta_1 \|[\![\mu]\!]\|_{H^{1/2}_{[\![\cdot]\!]}(\Gamma_c)}. \tag{17}$$

From definition (16), and using (17) we have for $\beta_2 > 1$ the following

$$\frac{1}{\beta_2}\|r_\gamma\|_{H^{-1/2}_{[\![\cdot]\!]}(\Gamma_c)} < \sup_{\substack{[\![\mu]\!] \in H^{1/2}_{[\![\cdot]\!]}(\Gamma_c) \\ [\![\mu]\!] \neq 0}} \frac{\displaystyle\int_{\Gamma_c} r_\gamma [\![\mu]\!] \, \mathrm{d}\Gamma}{\|[\![\mu]\!]\|_{H^{1/2}_{[\![\cdot]\!]}(\Gamma_c)}} \leq \beta_1 \sup_{\substack{\psi \in \mathcal{W}_d \\ [\![\mu]\!] = \psi_1(L) - \psi_{2|\Gamma_c} \\ \psi_1(L) \neq \psi_{2|\Gamma_c}}} \frac{\displaystyle\int_{\Gamma_c} r_\gamma [\![\mu]\!] \, \mathrm{d}\Gamma}{\|\psi\|_{\mathcal{W}_d}}, \tag{18}$$

and (15) follows with $\beta_0 = \frac{1}{\beta_1 \beta_2} > 0$.

It is worthwhile to show the theoretical consequences of considering different values of γ for this particular case. The general situation gives, from variational formulation (6), the following Euler–Lagrange equations

$$\begin{cases} -k\dfrac{\partial}{\partial z}\left(A(z)\dfrac{\partial \theta_1}{\partial z}\right) = \bar{f} & \text{in } (0,L), \\ -k\triangle\theta_2 = f & \text{in } \Omega_2, \\ k\nabla\theta_2 \cdot \mathbf{n}_2 = 0 & \text{on } \Gamma_{L_2}, \\ -k\dfrac{\partial \theta_1}{\partial z} = \gamma r_1 + (1-\gamma)\dfrac{1}{A_c}\displaystyle\int_{\Gamma_c} r_2 \, \mathrm{d}\Gamma & \text{in } z = L, \\ -k\nabla\theta_2 \cdot \mathbf{n}_1 = \gamma r_1 + (1-\gamma) r_2 & \text{on } \Gamma_c, \\ \gamma\left[\theta_1 - \dfrac{1}{A_c}\displaystyle\int_{\Gamma_c} \theta_2 \, \mathrm{d}\Gamma\right] = 0 & \text{in } z = L, \\ (1-\gamma)\Big[\theta_1 - \theta_2\Big] = 0 & \text{on } \Gamma_c. \end{cases} \tag{19}$$

The set of equations (19) clearly depicts the role of the parameter γ. In fact, at least from the theoretical point of view, the value of γ is important since it determines the sense in which equations $(19)_4$–$(19)_7$ are satisfied.

For example with $\gamma = 1$ we have the following problem

$$\begin{cases} -k\dfrac{\partial}{\partial z}\left(A(z)\dfrac{\partial\theta_1}{\partial z}\right) = \bar{f} & \text{in } (0,L), \\ -k\triangle\theta_2 = f & \text{in } \Omega_2, \\ k\nabla\theta_2\cdot\mathbf{n}_2 = 0 & \text{on } \Gamma_{L_2}, \\ k\dfrac{\partial\theta_1}{\partial z} = k\nabla\theta_2\cdot\mathbf{n}_1 & \text{on } \Gamma_c, \\ \theta_1 = \dfrac{1}{A_c}\displaystyle\int_{\Gamma_c}\theta_2\ \mathrm{d}\Gamma & \text{in } z = L. \end{cases} \tag{20}$$

In the above set of equations it is possible to see that the heat flux across Γ_c is continuous (see equation $(20)_4$), whereas the temperature is actually a discontinuous field (see equation $(20)_5$). Notice also that for this situation we have $r_1 = -k\frac{\partial\theta_1}{\partial z}(L) = -k(\nabla\theta_2\cdot\mathbf{n}_1)_{|\Gamma_c}$, and hence $\nabla\theta_2\cdot\mathbf{n}_1$ is constant on Γ_c.

The case $\gamma = 0$ leads to

$$\begin{cases} -k\dfrac{\partial}{\partial z}\left(A(z)\dfrac{\partial\theta_1}{\partial z}\right) = \bar{f} & \text{in } (0,L), \\ -k\triangle\theta_2 = f & \text{in } \Omega_2, \\ k\nabla\theta_2\cdot\mathbf{n}_2 = 0 & \text{on } \Gamma_{L_2}, \\ k\dfrac{\partial\theta_1}{\partial z} = \dfrac{1}{A_c}\displaystyle\int_{\Gamma_c}k\nabla\theta_2\cdot\mathbf{n}_1\ \mathrm{d}\Gamma & \text{in } z = L, \\ \theta_1 = \theta_2 & \text{on } \Gamma_c. \end{cases} \tag{21}$$

Contrariwise, for this situation we obtain a continuous temperature field (see equation $(21)_5$) while the heat flux across Γ_c is the quantity that remains discontinuous (see equation $(21)_4$). In this case we have $r_2 = -k(\nabla\theta_2\cdot\mathbf{n}_1)_{|\Gamma_c}$ and $-k\frac{\partial\theta_1}{\partial z}(L) = \frac{1}{A_c}\int_{\Gamma_c} r_2\ \mathrm{d}\Gamma$.

Observe that there exists a reciprocity relationship between cases at both extreme values of γ. In effect, for the case $\gamma = 0$ we obtain a situation in which the continuity in θ is actually enforced in a point–wise sense. As a counterpart we only recover the continuity of the mean value for the heat flow (see equation $(21)_4$). Conversely, with $\gamma = 1$ we have ensured the continuity for the heat flux in a point–wise sense (actually in a weak sense within the variational statement), while in this case we only recover the continuity for the mean value of the temperature (see equation $(20)_5$). Nonetheless, in spite of the differences commented, we see that always we attain a well–posed problem for any choice of γ.

Moreover, from the computational point of view and in the context of an iterative splitting between 1D and 3D computations, the set of equations (20) and (21) acquire a clearer meaning. In fact, for the system (20) we have that the 1D model feeds the 3D model with a constant Neumann boundary condition (equation $(20)_4$), while the 3D model provides the 1D model with a Dirichlet boundary condition (equation $(20)_5$). On the other hand, for the system (21) the opposite situation occurs since the 1D model furnishes the 3D model with a constant Dirichlet boundary condition (equation $(21)_5$), while the 3D model feeds the 1D model with a Neumann boundary condition (equation $(21)_4$).

The opposite situations referred to in the above arise only in the particular case when a kinematical assumption over a portion of the domain Ω has been considered. In the case of no kinematical constraints, as the situation given by problem (3), we do not discern this reciprocity, and the kinematical restrictions appear only at the discrete counterpart of the problem when the corresponding, possibly non–matching, discretizations for Ω_1 and Ω_2 are given. In this case of non–matching meshes, the formulation is closely related to those domain-decomposition techniques, since in this case this incompatibility entails different kinematics at the discrete level for both domains, and therefore the same ideas apply. For the extreme values of γ the formulation can be then understood as a method based on the Steklov–Poincaré operator, where the mapping is inverted when passing from $\gamma = 1$ to $\gamma = 0$ or viceversa.

3 Variational formulation for fluid flow in compliant vessels

In this section we address the problem of the flow of an incompressible fluid within a compliant domain.

Let us consider an arbitrary compliant vessel given by the domain $\Omega \subset \mathbb{R}^{n_d}$, $(n_d = 2, 3)$ as shown in Figure 3 with boundary Γ decomposed in the part corresponding to the wall, namely Γ_w, and the corresponding ones to each input–output face, namely Γ_i. Thus we have $\Gamma = \Gamma_w \cup \left(\cup_{i=1}^{N_s} \Gamma_i\right)$, where N_s is the total number of faces for which we have interchange of mass by setting corresponding Dirichlet conditions. Let us suppose a no–slip condition over Γ_w, even so, and for simplicity in the reduction of the model over a portion of the domain, say Ω_1, performed in the next section, we consider the corresponding traction over the boundary of Ω_1 corresponding to the wall, say Γ_{w1}, that accomplishes the equilibrium. This traction will be given consistent with the structural model. The problem can be stated in an Eulerian framework, or in an arbitrary Lagrangian–Eulerian framework as well [18].

Within the context of an ALE variational approach, the flow of an incompressible fluid in a compliant vessel, like the one shown in Figure 3, can be

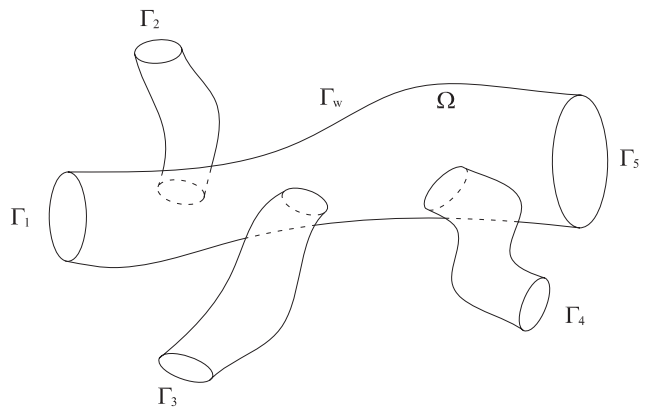

Fig. 3. Arbitrary compliant vessel.

formulated as follows: *for every* $t \in (0, T)$, *find* $(\mathbf{u}, p) \in \mathcal{U} \times \mathcal{P}$ *such that*

$$\int_\Omega \rho \left.\frac{\partial \mathbf{u}}{\partial t}\right|_{\mathbf{Y}} \cdot \mathbf{v} \, \mathrm{d}\mathbf{x} + \int_\Omega \rho \nabla \mathbf{u}(\mathbf{u} - \mathbf{w}) \cdot \mathbf{v} \, \mathrm{d}\mathbf{x} - \int_\Omega p \operatorname{div} \mathbf{v} \, \mathrm{d}\mathbf{x} + \int_\Omega \boldsymbol{\sigma}_D(\mathbf{u}) \cdot \boldsymbol{\varepsilon}(\mathbf{v}) \, \mathrm{d}\mathbf{x} - \int_\Omega \mathbf{f} \cdot \mathbf{v} \, \mathrm{d}\mathbf{x} - \int_{\Gamma_{w1}} \mathbf{t}_w \cdot \mathbf{v} \, \mathrm{d}\Gamma = 0 \qquad \forall \mathbf{v} \in \mathcal{V}, \quad (22a)$$

$$\int_\Omega \rho \operatorname{div} \mathbf{u} \, q \, \mathrm{d}\mathbf{x} = 0 \qquad \forall q \in \mathcal{Q}, \quad (22b)$$

with proper initial conditions. Here, $\mathbf{u}$ is the velocity field, $\mathbf{v}$ is an admissible variation of the velocity field, $\mathbf{w}$ is the velocity of the ALE frame of reference, $\boldsymbol{\sigma} = -p\mathbf{I} + \boldsymbol{\sigma}_D(\mathbf{u})$ is the Cauchy stress tensor where p is the pressure field and $\boldsymbol{\sigma}_D(\mathbf{u})$ is its deviatoric part, q is an admissible variation of the pressure field, ρ is the fluid density, $\mathbf{f}$ is a volume force, $\mathbf{t}_w$ is the traction vector over the vessel wall corresponding to Ω_1, $\mathbf{n}$ is the corresponding outward unit normal vector and $\boldsymbol{\varepsilon}(\mathbf{v})$ is the strain rate tensor associated to the admissible variation $\mathbf{v}$, that is $\boldsymbol{\varepsilon}(\mathbf{v}) = \frac{1}{2}(\nabla \mathbf{v} + (\nabla \mathbf{v})^T)$. Also, $\left.\frac{\partial(\cdot)}{\partial t}\right|_{\mathbf{Y}}$ denotes the derivative when fixing ALE coordinates $\mathbf{Y}$, also $\mathbf{f}$ and $\mathbf{t}_w$ are such that expression (22a) makes sense. After a little of calculus it is possible to obtain a conservative form for the mass conservation equation as follows

$$\frac{\mathrm{d}}{\mathrm{d}t} \int_\Omega \rho q \, \mathrm{d}\mathbf{x} - \int_\Omega \rho(\mathbf{u} - \mathbf{w}) \cdot \nabla q \, \mathrm{d}\mathbf{x} + \int_\Gamma \rho(\mathbf{u} - \mathbf{w}) \cdot \mathbf{n} \, q \, \mathrm{d}\Gamma = 0 \quad \forall q \in \mathcal{Q}. \quad (23)$$

From such a conservative expression it is more direct to reduce the problem to a 1D model, as it will be done in the next section. Also, in this problem we consider null mass flux across the vessel wall Γ_w.

The set $\mathcal{U} \times \mathcal{P}$ establishes regularity and essential boundary conditions such that problem (22) is well–posed. In this work we do not present existence nor uniqueness results for the extended variational formulation of the Navier–Stokes problem. Classical results concerning the well–posedness of this prob-

lem can be found in [14,15]. Therefore, variational formulation (22) is well stated only when working with fields $(\mathbf{u}, p)$ being regular enough in Ω, in the sense that the pair must be in $\mathcal{U} \times \mathcal{P}$. It is usual to consider for formulation (23) that

$$\begin{aligned} \mathcal{U} &= \{\mathbf{u} \in [H^1(\Omega)]^{n_d};\ \mathbf{u}_{|\Gamma_i} = \bar{\mathbf{u}}_i \text{ on } \Gamma_i,\ i = 1, \ldots, N_s; \\ &\qquad\qquad\qquad\qquad\qquad\qquad\qquad\qquad \mathbf{u}_{|\Gamma_{w2}} = \mathbf{w}_{|\Gamma_{w2}}\}, \\ \mathcal{P} &= L^2(\Omega), \end{aligned} \tag{24}$$

while we demand additional regularity for field p if we work with the conservative form of the mass conservation given by (23). As seen above, the no–slip condition over $\Gamma_{w2} = \Gamma_w \setminus \Gamma_{w1}$ is incorporated in the set $\mathcal{U}$.

4 Extended variational formulation for fluid flow in compliant vessels

In order to recast the problem of coupling 3D with 1D models for modelling the blood flow in large arteries we turn to introducing different kinematics for each part of a given domain, that will correspond to the 3D and 1D models. In this sense, we interpret that discontinuities may occur at the coupling interface as a result of the dissimilarity between the kinematics of each model, in the same way as done in the heat transfer problem. The goal of this section is to introduce an extended governing variational principle that allows us to establish different kinematics for different parts of a given split domain, and thus to manage the mentioned discontinuities in the involved fields.

4.1 Statement of the problem

For the sake of simplicity in illustrating the problem we work with the simple domain already shown in Figure 2. Recall that Γ_c is an internal boundary of Ω that splits the domain as being $\Omega = \Omega_1 \cup \Omega_2 \cup \Gamma_c$, with boundaries Γ_1 and Γ_2 respectively. Thus, we have $\Gamma_c = \Gamma_1 \cap \Gamma_2$. The vessel wall is now decomposed as $\Gamma_w = \Gamma_{w1} \cup \Gamma_{w2}$, and we also refer to Γ_A and Γ_B as Γ_{in} and Γ_{out} respectively. Then we have $\Gamma_1 = \Gamma_{\text{in}} \cup \Gamma_{w1} \cup \Gamma_c$ and $\Gamma_2 = \Gamma_{\text{out}} \cup \Gamma_{w2} \cup \Gamma_c$. As mentioned, we will work with different kinematics on each part of Ω, say Ω_1 and Ω_2, proceeding analogously to that performed for the heat transfer problem.

We shall also suppose, without loss of generality, that the problem is such that has proper Dirichlet boundary conditions at both extremes of domain Ω, that is at Γ_{in} and Γ_{out}. In this way, the analysis will be focused where discontinuities occur, that is on Γ_c.

Let us consider over Ω_i function set $\mathcal{U}_i \times \mathcal{P}_i$, $i = 1, 2$, that will characterize the corresponding model. No assumptions are made concerning conditions at interface Γ_c. Let us take the velocity $\mathbf{w}$ of the ALE frame of reference such that $\mathbf{w} \cdot \mathbf{n} = 0$ on Γ_{in}, Γ_{out} and Γ_c. Recall that over Γ_{w1} the Neumann boundary condition is used while over Γ_{w2} the Dirichlet boundary condition is considered.

Let us write $\mathbf{u} = (\mathbf{u}_1, \mathbf{u}_2)$, with $\mathbf{u}_1 \in \mathcal{U}_1$ and $\mathbf{u}_2 \in \mathcal{U}_2$. In the same way it is $p = (p_1, p_2)$ with $p_1 \in \mathcal{P}_1$ and $p_2 \in \mathcal{P}_2$. Then we have $\mathcal{U}_d = \mathcal{U}_1 \times \mathcal{U}_2$ and $\mathcal{P}_d = \mathcal{P}_1 \times \mathcal{P}_2$. We will focus our attention upon the momentum equation. Thus, the resulting extended variational principle for the momentum balance is the following

$$
\begin{aligned}
&\int_{\Omega_1} \rho \left.\frac{\partial \mathbf{u}_1}{\partial t}\right|_{\mathbf{Y}} \cdot \mathbf{v}_1 \, \mathrm{d}\mathbf{x} + \int_{\Omega_1} \rho \nabla \mathbf{u}_1 (\mathbf{u}_1 - \mathbf{w}) \cdot \mathbf{v}_1 \, \mathrm{d}\mathbf{x} \\
&- \int_{\Omega_1} p_1 \operatorname{div} \mathbf{v}_1 \, \mathrm{d}\mathbf{x} + \int_{\Omega_1} \boldsymbol{\sigma}_D(\mathbf{u}_1) \cdot \boldsymbol{\varepsilon}(\mathbf{v}_1) \, \mathrm{d}\mathbf{x} - \int_{\Omega_1} \mathbf{f} \cdot \mathbf{v}_1 \, \mathrm{d}\mathbf{x} - \int_{\Gamma_{w1}} \mathbf{t}_w \cdot \mathbf{v}_1 \, \mathrm{d}\Gamma \\
&\qquad + \int_{\Omega_2} \rho \left.\frac{\partial \mathbf{u}_2}{\partial t}\right|_{\mathbf{Y}} \cdot \mathbf{v}_2 \, \mathrm{d}\mathbf{x} + \int_{\Omega_2} \rho \nabla \mathbf{u}_2 (\mathbf{u}_2 - \mathbf{w}) \cdot \mathbf{v}_2 \, \mathrm{d}\mathbf{x} \\
&\qquad - \int_{\Omega_2} p_2 \operatorname{div} \mathbf{v}_2 \, \mathrm{d}\mathbf{x} + \int_{\Omega_2} \boldsymbol{\sigma}_D(\mathbf{u}_2) \cdot \boldsymbol{\varepsilon}(\mathbf{v}_2) \, \mathrm{d}\mathbf{x} - \int_{\Omega_2} \mathbf{f} \cdot \mathbf{v}_2 \, \mathrm{d}\mathbf{x} \\
&+ \int_{\Gamma_c} [\gamma \mathbf{r}_1 + (1-\gamma)\mathbf{r}_2] \cdot (\mathbf{v}_2 - \mathbf{v}_1) \, \mathrm{d}\Gamma + \int_{\Gamma_c} [\gamma \mathbf{s}_1 + (1-\gamma)\mathbf{s}_2] \cdot (\mathbf{u}_2 - \mathbf{u}_1) \, \mathrm{d}\Gamma = 0 \\
&\qquad \forall (\mathbf{v}, \mathbf{s}_1, \mathbf{s}_2) \in \mathcal{V}_d \times \mathcal{Z}_1 \times \mathcal{Z}_2, \quad (25)
\end{aligned}
$$

where $\mathbf{r}_1 \in \mathcal{Z}_1$ and $\mathbf{r}_2 \in \mathcal{Z}_2$ are the counterpart variables of r_1 and r_2 present in the heat transfer problem, with variations $\mathbf{s}_1$ and $\mathbf{s}_2$ respectively. Also we have $\mathbf{v} = (\mathbf{v}_1, \mathbf{v}_2) \in \mathcal{V}_d = \mathcal{V}_1 \times \mathcal{V}_2$.

Notice that formulation (25) could have also been generalized for the situation with several faces Γ_{ci}, $i = 1, \ldots, N_c$ where discontinuities can occur. This generalization is straightforward and was omitted here for the sake of brevity.

Now let us suppose that the field $\mathbf{u}_1$ is

$$
\mathbf{u}_1 = \bar{u}(z, t)\mathbf{e}_z, \tag{26}
$$

where $\mathbf{e}_z$ is the unit axial vector in the direction of the normal to a generic transversal plane defined by coordinates x, y (see Figure 2). Thus, admissible variations of $\mathbf{u}_1$ have the form $\mathbf{v}_1 = \bar{v}\mathbf{e}_z$. With this choice we have that

$$
\begin{aligned}
p_1 &= \bar{p}(z, t), \\
\mathbf{r}_1 &= \bar{r}_1(t)\mathbf{e}_z,
\end{aligned} \tag{27}
$$

and then the admissible variations of p_1 and $\mathbf{r}_1$ are denoted by $\bar{q}$ and $\mathbf{s}_1 = \bar{s}_1\mathbf{e}_z$ respectively. Over Ω_1 it is considered that $\mathbf{w} \cdot \mathbf{e}_z = 0$. Therefore, we have $\frac{\partial(\cdot)}{\partial t} =$

$\frac{\partial(\cdot)}{\partial t}|_z$, that is, when the z coordinate is fixed the time derivatives coincide.

Therefore, introducing assumption (26) together with (27) into expression (25), integrating over the transversal area Γ_z, namely $A(z,t)$, and considering the corresponding form of the admissible variations we obtain, after a little of work, the following expression

$$\begin{aligned}
\int_0^L \rho A \frac{\partial \bar{u}}{\partial t}\bar{v}\ \mathrm{d}z + \int_0^L \rho A \bar{u}\frac{\partial \bar{u}}{\partial z}\bar{v}\ \mathrm{d}z - \int_0^L A\bar{p}\frac{\partial \bar{v}}{\partial z}\ \mathrm{d}z + \int_0^L \bar{\sigma}_D(\bar{u})\frac{\partial \bar{v}}{\partial z}\ \mathrm{d}z \\
- \int_0^L \oint_{C_z} t_w^z \bar{v}\ \mathrm{d}l\,\mathrm{d}z - \int_0^L f^z \bar{v}\ \mathrm{d}z \\
+ \int_{\Omega_2} \rho \left.\frac{\partial \mathbf{u}_2}{\partial t}\right|_{\mathbf{Y}} \cdot \mathbf{v}_2\ \mathrm{d}\mathbf{x} + \int_{\Omega_2} \rho \nabla \mathbf{u}_2(\mathbf{u}_2 - \mathbf{w})\cdot \mathbf{v}_2\ \mathrm{d}\mathbf{x} \\
- \int_{\Omega_2} p_2 \operatorname{div} \mathbf{v}_2\ \mathrm{d}\mathbf{x} + \int_{\Omega_2} \boldsymbol{\sigma}_D(\mathbf{u}_2)\cdot \boldsymbol{\varepsilon}(\mathbf{v}_2)\ \mathrm{d}\mathbf{x} - \int_{\Omega_2} \mathbf{f}\cdot \mathbf{v}_2\ \mathrm{d}\mathbf{x} \\
+ \int_{\Gamma_c} [\gamma \bar{r}_1(\mathbf{v}_2\cdot \mathbf{n}_1 - \bar{v}) + (1-\gamma)\mathbf{r}_2\cdot(\mathbf{v}_2 - \bar{v}\mathbf{n}_1)]\ \mathrm{d}\Gamma \\
+ \int_{\Gamma_c} [\gamma \bar{s}_1(\mathbf{u}_2\cdot \mathbf{n}_1 - \bar{u}) + (1-\gamma)\mathbf{s}_2\cdot(\mathbf{u}_2 - \bar{u}\mathbf{n}_1)]\ \mathrm{d}\Gamma = 0 \\
\forall (\mathbf{v}, \mathbf{s}_1, \mathbf{s}_2) \in \mathcal{V}_d \times \mathcal{Z}_1 \times \mathcal{Z}_2, \quad (28)
\end{aligned}$$

where $f^z = \int_{\Gamma_z} \mathbf{f}\cdot\mathbf{e}_z\ \mathrm{d}\Gamma$, $\bar{\sigma}_D(\bar{u}) = \int_{\Gamma_z} \boldsymbol{\sigma}_D(\mathbf{u}_1)\cdot(\mathbf{e}_z\otimes\mathbf{e}_z)\ \mathrm{d}\Gamma$, C_z is the boundary curve of the generic transversal section $A(z,t)$ and t_w^z is the component of $\mathbf{t}_w$ in the $\mathbf{e}_z$ direction. Also notice that over Γ_c we have $\mathbf{e}_z = \mathbf{n}_1 = -\mathbf{n}_2$. It is not difficult to see that

$$\oint_{C_z} t_w^z\ \mathrm{d}l = \bar{p}\frac{\partial A}{\partial z} + t_D^z(\bar{u}), \tag{29}$$

where $t_D^z(\bar{u}) = \oint_{C_z} \boldsymbol{\sigma}_D(\mathbf{u}_1)\cdot(\mathbf{e}_z\otimes\mathbf{n}_w)\ \mathrm{d}l$ and $\mathbf{n}_w$ is the outward unit normal vector of the boundary corresponding to the wall Γ_{w1}. From expressions (28) and (29) it can be observed that proper constitutive behaviors will have to be given for the generalized quantities $\bar{\sigma}_D$ and t_D^z in terms of the velocity $\bar{u}$. Introducing (29) in equation (28) follows that

$$\begin{aligned}
\int_0^L \rho A \frac{\partial \bar{u}}{\partial t}\bar{v}\ \mathrm{d}z + \int_0^L \rho A \bar{u}\frac{\partial \bar{u}}{\partial z}\bar{v}\ \mathrm{d}z - \int_0^L A\bar{p}\frac{\partial \bar{v}}{\partial z}\ \mathrm{d}z + \int_0^L \bar{\sigma}_D(\bar{u})\frac{\partial \bar{v}}{\partial z}\ \mathrm{d}z \\
- \int_0^L \bar{p}\frac{\partial A}{\partial z}\bar{v}\,\mathrm{d}z - \int_0^L t_D^z(\bar{u})\bar{v}\ \mathrm{d}z - \int_0^L f^z \bar{v}\ \mathrm{d}z \\
+ \int_{\Omega_2} \rho \left.\frac{\partial \mathbf{u}_2}{\partial t}\right|_{\mathbf{Y}} \cdot \mathbf{v}_2\ \mathrm{d}\mathbf{x} + \int_{\Omega_2} \rho \nabla \mathbf{u}_2(\mathbf{u}_2 - \mathbf{w})\cdot \mathbf{v}_2\ \mathrm{d}\mathbf{x} \\
- \int_{\Omega_2} p_2 \operatorname{div} \mathbf{v}_2\ \mathrm{d}\mathbf{x} + \int_{\Omega_2} \boldsymbol{\sigma}_D(\mathbf{u}_2)\cdot \boldsymbol{\varepsilon}(\mathbf{v}_2)\ \mathrm{d}\mathbf{x} - \int_{\Omega_2} \mathbf{f}\cdot \mathbf{v}_2\ \mathrm{d}\mathbf{x} \\
+ \int_{\Gamma_c} [\gamma \bar{r}_1(\mathbf{v}_2\cdot \mathbf{n}_1 - \bar{v}) + (1-\gamma)\mathbf{r}_2\cdot(\mathbf{v}_2 - \bar{v}\mathbf{n}_1)]\ \mathrm{d}\Gamma \\
+ \int_{\Gamma_c} [\gamma \bar{s}_1(\mathbf{u}_2\cdot \mathbf{n}_1 - \bar{u}) + (1-\gamma)\mathbf{s}_2\cdot(\mathbf{u}_2 - \bar{u}\mathbf{n}_1)]\ \mathrm{d}\Gamma = 0 \\
\forall (\mathbf{v}, \mathbf{s}_1, \mathbf{s}_2) \in \mathcal{V}_d \times \mathcal{Z}_1 \times \mathcal{Z}_2. \quad (30)
\end{aligned}$$

Concerning the mass conservation, from equation (23) we have

$$\frac{\mathrm{d}}{\mathrm{d}t}\int_{\Omega_1}\rho q_1\ \mathrm{d}\mathbf{x}-\int_{\Omega_1}\rho(\mathbf{u}_1-\mathbf{w})\cdot\nabla q_1\ \mathrm{d}\mathbf{x}+\int_{\Gamma_1}\rho(\mathbf{u}_1-\mathbf{w})\cdot\mathbf{n}_1\,q_1\ \mathrm{d}\Gamma+ \\ \frac{\mathrm{d}}{\mathrm{d}t}\int_{\Omega_2}\rho q_2\ \mathrm{d}\mathbf{x}-\int_{\Omega_2}\rho(\mathbf{u}_2-\mathbf{w})\cdot\nabla q_2\ \mathrm{d}\mathbf{x}+\int_{\Gamma_2}\rho(\mathbf{u}_2-\mathbf{w})\cdot\mathbf{n}_2\,q_2\ \mathrm{d}\Gamma \\ =0\quad\forall q\in\mathcal{Q}_d,\quad(31)$$

where $q=(q_1,q_2)\in\mathcal{Q}_d=\mathcal{Q}_1\times\mathcal{Q}_2$. From this expression it can be easily verified, by introducing assumption (26) together with (27), that

$$\int_0^L\rho\frac{\partial A}{\partial t}\bar{q}\ \mathrm{d}z+\int_0^L\rho\frac{\partial(A\bar{u})}{\partial z}\bar{q}\ \mathrm{d}z+\int_{\Omega_2}\rho\,\mathrm{div}\,\mathbf{u}_2q_2\ \mathrm{d}\mathbf{x}=0\qquad\forall q\in\mathcal{Q}_d.\quad(32)$$

4.2 Euler equations

Let us obtain the Euler equations related to variational expression (30) and (32). Recall that over Γ_{in} and Γ_{out} we impose a Dirichlet boundary condition. Thus, in the sense of distributions it is possible to write from (30) the following

$$\int_0^L\left[\rho A\frac{\partial\bar{u}}{\partial t}+\rho A\bar{u}\frac{\partial\bar{u}}{\partial z}+\frac{\partial(A\bar{p})}{\partial z}-\frac{\partial}{\partial z}\big(\bar{\sigma}_D(\bar{u})\big)-\bar{p}\frac{\partial A}{\partial z}-t_D^z(\bar{u})-f^z\right]\bar{v}\ \mathrm{d}z \\ +\int_{\Omega_2}\left[\rho\frac{\partial\mathbf{u}_2}{\partial t}\bigg|_{\mathbf{Y}}+\rho\nabla\mathbf{u}_2(\mathbf{u}_2-\mathbf{w})+\nabla p_2-\mathrm{div}\,\boldsymbol{\sigma}_D(\mathbf{u}_2)-\mathbf{f}\right]\cdot\mathbf{v}_2\ \mathrm{d}\mathbf{x} \\ \left[-A_c\bar{p}+A_c\bar{\sigma}_D(\bar{u})-\left(\gamma A_c\bar{r}_1+(1-\gamma)\int_{\Gamma_c}\mathbf{r}_2\cdot\mathbf{n}_1\ \mathrm{d}\Gamma\right)\right]\bar{v}\bigg|_{z=L} \\ +\int_{\Gamma_c}\left[(-p_2\mathbf{I}+\boldsymbol{\sigma}_D(\mathbf{u}_2))\mathbf{n}_2+\gamma\bar{r}_1\mathbf{n}_1+(1-\gamma)\mathbf{r}_2\right]\cdot\mathbf{v}_2\ \mathrm{d}\Gamma \\ +\gamma\bar{s}_1\left[-(A_c\bar{u})|_{z=L}+\int_{\Gamma_c}\mathbf{u}_2\cdot\mathbf{n}_1\ \mathrm{d}\Gamma\right]+(1-\gamma)\left[\int_{\Gamma_c}(\mathbf{u}_2-\bar{u}\mathbf{n}_1)\cdot\mathbf{s}_2\ \mathrm{d}\Gamma\right]=0 \\ \forall(\mathbf{v},\mathbf{s}_1,\mathbf{s}_2)\in\mathcal{V}_d\times\mathcal{Z}_1\times\mathcal{Z}_2,\quad(33)$$

where A_c is the value of the area at Γ_c. Also, from (32) we have

$$\int_0^L\rho\left[\frac{\partial A}{\partial t}+\frac{\partial(A\bar{u})}{\partial z}\right]\bar{q}\ \mathrm{d}z+\int_{\Omega_2}\rho\,\mathrm{div}\,\mathbf{u}_2q_2\ \mathrm{d}\mathbf{x}=0\qquad\forall q\in\mathcal{Q}_d.\quad(34)$$

Hence we recast the following nonlinear system of Euler–Lagrange equations

$$\rho A\frac{\partial\bar{u}}{\partial t}+\rho A\bar{u}\frac{\partial\bar{u}}{\partial z}=-A\frac{\partial\bar{p}}{\partial z}+\frac{\partial}{\partial z}\big(\bar{\sigma}_D(\bar{u})\big) \\ +t_D^z(\bar{u})+f^z\qquad\text{in }(0,L)\times(0,T),\quad(35a)$$

$$\rho \frac{\partial \mathbf{u}_2}{\partial t}\bigg|_{\mathbf{Y}} + \rho \nabla \mathbf{u}_2(\mathbf{u}_2 - \mathbf{w}) = -\nabla p_2 + \operatorname{div} \boldsymbol{\sigma}_D(\mathbf{u}_2) + \mathbf{f} \quad \text{in } \Omega_2 \times (0,T), \tag{35b}$$

$$\frac{\partial A}{\partial t} + \frac{\partial (A\bar{u})}{\partial z} = 0 \quad \text{in } (0,L) \times (0,T), \tag{35c}$$

$$\operatorname{div} \mathbf{u}_2 = 0 \quad \text{in } \Omega_2 \times (0,T), \tag{35d}$$

$$\gamma \bar{r}_1 + (1-\gamma) \frac{1}{A_c} \int_{\Gamma_c} \mathbf{r}_2 \cdot \mathbf{n}_1 \, \mathrm{d}\Gamma = -\bar{p} + \bar{\sigma}_D(\bar{u}) \quad \text{in } \{z = L\} \times (0,T), \tag{35e}$$

$$\gamma \bar{r}_1 \mathbf{n}_1 + (1-\gamma)\mathbf{r}_2 = [-p_2 \mathbf{I} + \boldsymbol{\sigma}_D(\mathbf{u}_2)]\mathbf{n}_1 \quad \text{on } \Gamma_c \times (0,T), \tag{35f}$$

$$\gamma \left[A_c \bar{u} - \int_{\Gamma_c} \mathbf{u}_2 \cdot \mathbf{n}_1 \, \mathrm{d}\Gamma \right] = 0 \quad \text{in } \{z = L\} \times (0,T), \tag{35g}$$

$$(1-\gamma)\Big[\mathbf{u}_2 - \bar{u}\mathbf{n}_1\Big] = 0 \quad \text{on } \Gamma_c \times (0,T), \tag{35h}$$

where point $z = L$ corresponds to face Γ_c (see Figure 2).

As in the heat transfer problem, when $\gamma = 1$ we obtain, from equations (35e)–(35f), the following

$$\begin{aligned} \bar{r}_1 &= -\bar{p} + \bar{\sigma}_D(\bar{u}) && \text{in } \{z = L\} \times (0,T), \\ \bar{r}_1 \mathbf{n}_1 &= [-p_2 \mathbf{I} + \boldsymbol{\sigma}_D(\mathbf{u}_2)]\mathbf{n}_1 && \text{on } \Gamma_c \times (0,T). \end{aligned} \tag{36}$$

Therefore, combining these expressions and from equation (35g) we finally arrive to

$$[-p_2 \mathbf{I} + \boldsymbol{\sigma}_D(\mathbf{u}_2)]\mathbf{n}_1 = [-\bar{p} + \bar{\sigma}_D(\bar{u})]\mathbf{n}_1 \quad \text{on } \Gamma_c \times (0,T), \tag{37a}$$

$$A_c \bar{u} = \int_{\Gamma_c} \mathbf{u}_2 \cdot \mathbf{n}_1 \, \mathrm{d}\Gamma \quad \text{in } \{z = L\} \times (0,T). \tag{37b}$$

As in the heat transfer problem, for $\gamma = 1$ we obtain that the normal traction on Γ_c is continuous (see equation (37a)) while the velocity field is discontinuous (see equation (37b)).

On the other hand, if $\gamma = 0$ we arrive, in a similar manner, to the following expressions

$$\frac{1}{A_c} \int_{\Gamma_c} [-p_2 + \boldsymbol{\sigma}_D(\mathbf{u}_2) \cdot (\mathbf{n}_1 \otimes \mathbf{n}_1)] \, \mathrm{d}\Gamma = -\bar{p} + \bar{\sigma}_D(\bar{u}) \quad \text{in } \{z = L\} \times (0,T), \tag{38a}$$

$$\mathbf{u}_2 = \bar{u}\mathbf{n}_1 \quad \text{on } \Gamma_c \times (0,T), \tag{38b}$$

where, contrarily to the previous case, the velocity field is continuous (see equation (38b)) whereas the normal traction is discontinuous on Γ_c (see equation (38a)).

Also, and in the context of a domain decomposition technique when approximating the problem, it is worth noticing that the governing variational principle stated in this work leads to those formulations mentioned in [12,38], that are aimed at handling problems with defective boundary conditions. Note that in this case we have extended the formulation for a larger class of problems. Indeed, consider $\gamma = 1$. On one hand we can assume that $Q_c = A_c\bar{u}$ is known (we are in this case not interested in what happens in domain Ω_1) and then we have the *prescribed flow rate problem* treated in references [12,38]. In this case $\bar{r}_1$ represents the associated Lagrange multiplier that enforces the given flow rate. On the other hand, if what we know is $\bar{r}_1 = -\bar{p}$ (again we are forgetting what occurs in Ω_1) then we recover the so called *mean pressure problem*, and the flow rate Q_c is a mere consequence.

Fluid over domain Ω_2 is hereafter considered as Newtonian, that is

$$\boldsymbol{\sigma}_D(\mathbf{u}_2) = 2\mu\boldsymbol{\varepsilon}(\mathbf{u}_2), \tag{39}$$

while for domain Ω_1 the following generalized constitutive behaviors are considered

$$\begin{aligned} \bar{\sigma}_D(\bar{u}) &= 0, \\ t_D^z(\bar{u}) &= -8\pi\mu\bar{u}. \end{aligned} \tag{40}$$

Although the constitutive laws given in the above coincide with the case of a parabolic profile, no contradictions appear since the form of the profile is not being considered here. Actually, the question here is how to provide the forms of $\bar{\sigma}_D(\bar{u})$ and $t_D^z(\bar{u})$ so as to obtain good agreement between the mathematical model and experimental results. Then any choice of the constitutive behavior for the generalized stresses can be given provided acceptable results are obtained.

Remark 3 *As far as constitutive laws are concerned note that it is possible to establish different constitutive behaviors for both domains Ω_1 and Ω_2, since expressions $\bar{\sigma}_D(\bar{u})$, $t_D^z(\bar{u})$ and $\boldsymbol{\sigma}_D(\mathbf{u}_2)$ need not be in compliance with any compatibility condition between them.*

Therefore, using (40) the momentum equation (35a) results

$$\rho A\frac{\partial\bar{u}}{\partial t} + \rho A\bar{u}\frac{\partial\bar{u}}{\partial z} = -A\frac{\partial\bar{p}}{\partial z} - 8\pi\mu\bar{u} + f^z \qquad \text{in } (0,L)\times(0,T), \tag{41}$$

thus incorporating those classical frictional terms seen in the literature for the

1D model [1,17,27], whilst equation (35e) now is

$$\gamma \bar{r}_1 + (1-\gamma)\frac{1}{A_c}\int_{\Gamma_c} \mathbf{r}_2 \cdot \mathbf{n}_1 \, \mathrm{d}\Gamma = -\bar{p} \qquad \text{in } \{z = L\} \times (0, T). \tag{42}$$

Consequently, the general setting proposed here allowed us to obtain not only the equilibrium equations for both models, but also the corresponding coupling terms that are now naturally derived since they are implied within the governing variational principle.

Notice that when the set of equations (30)–(32), is intended to model the fully coupled fluid–structure interaction problem that arises in the context of hemodynamics, it must be complemented with appropriate relations characterizing the structural behavior of the vessel wall, as will be done in Section 5.

5 Approximate solutions

This section is devoted to present the approximation techniques in order to find approximate solutions for the problem treated in the previous section. Also, and in the first place, a discussion referring to the choice of the parameter γ is addressed.

5.1 On the choice of parameter γ

As could be seen in the previous section, the nature of the problem changes when varying the value of γ from 0 to 1. From the theoretical point of view the same problem is recovered when $\gamma \in (0, 1)$ since the Euler equations are the same. Moreover, the choice $\gamma = 1$, $\gamma \in (0, 1)$ or $\gamma = 0$ is not a relevant problem from the modelling point of view. Indeed, when using coupled models it is important to remark that no reliable solutions must be expected in the regions near the coupling interfaces due to the poor information that, in some sense, is provided by the reduced model. Then, the choice of γ should be made in order to simplify the computational implementation. It is obvious that when $\gamma \in [0, 1)$ the number of degrees of freedom is larger than for $\gamma = 1$. This shows an interesting feature of the latter case. Furthermore, it is emphasized by the fact that for the particular case of $\gamma = 1$ the system can be reduced when written in its canonical form as will be done later on.

Another important aspect is the numerical relevance that the parameter γ could have, mainly in the context of iterative segregated schemes. Concerning this, and anticipating some results, in the numerical experiments performed no differences appeared neither in the solutions nor in the convergence of

the coupling scheme when varying γ in the interval $[0,1)$. In addition, it was observed that the computational cost clearly increased.

For the reasons mentioned in the previous paragraph we continue hereafter with $\gamma = 1$. Certainly, the problem in terms of the Euler equations results the following

$$\rho A \frac{\partial \bar{u}}{\partial t} + \rho A \bar{u} \frac{\partial \bar{u}}{\partial z} = -A \frac{\partial \bar{p}}{\partial z} - 8\pi\mu\bar{u} + f^z \quad \text{in } (0,L)\times(0,T), \tag{43a}$$

$$\rho \left.\frac{\partial \mathbf{u}_2}{\partial t}\right|_{\mathbf{Y}} + \rho \nabla \mathbf{u}_2 (\mathbf{u}_2 - \mathbf{w}) = -\nabla p_2 + \mu \triangle \mathbf{u}_2 + \mathbf{f} \quad \text{in } \Omega_2 \times (0,T), \tag{43b}$$

$$\frac{\partial A}{\partial t} + \frac{\partial (A\bar{u})}{\partial z} = 0 \quad \text{in } (0,L)\times(0,T), \tag{43c}$$

$$\operatorname{div} \mathbf{u}_2 = 0 \quad \text{in } \Omega_2 \times (0,T), \tag{43d}$$

$$(-p_2 \mathbf{I} + 2\mu \boldsymbol{\varepsilon}(\mathbf{u}_2))\, \mathbf{n}_1 = -\bar{p}\, \mathbf{n}_1 \quad \text{on } \Gamma_c \times (0,T), \tag{43e}$$

$$A_c \bar{u} = \int_{\Gamma_c} \mathbf{u}_2 \cdot \mathbf{n}_1 \, \mathrm{d}\Gamma \quad \text{on } \Gamma_c \times (0,T). \tag{43f}$$

Equation (43e) stands for the continuity of the traction vector at Γ_c, while expression (43f) is the counterpart of the mass conservation at Γ_c.

As a final comment observe that in the particular situation of a rigid pipe modelled as a 3D–1D domain, for this case of $\gamma = 1$ we recover, just over the whole 3D domain and in the stationary case, the exact parabolic profile and the constant pressure gradient. For another choices of γ flat profiles at both coupling interfaces occur and therefore the well–known hydrodynamical development length is obtained. Actually, at the outlet we obtain a hydrodynamical de–development length.

5.2 Wall behavior and characteristics equations

Before introducing such a numerical scheme, it is necessary to specify the arterial wall behavior in order to characterize the derived fluid–structure interaction model. Accordingly, we choose a simple model such that corresponding counterpart expressions at both parts of the domain (3D and 1D parts) can be given in order to recover an analogous behavior at both sides of the coupling interfaces. Hence we will use the *independent ring model* [16,21,22] because of its simplicity and also because it leads to realistic results. The corresponding equations for both 1D and 3D domains are the following

$$\bar{p} = \bar{p}_0 + \frac{E\pi R_0 h}{A}\left(\sqrt{\frac{A}{A_0}} - 1\right) + \frac{k\pi R_0 h}{A}\frac{1}{2\sqrt{A_0 A}}\frac{\partial A}{\partial t} \quad \text{in } (0,L)\times(0,T), \tag{44a}$$

$$p_2 = p_{2_0} + \frac{Eh}{R_0^2}\zeta + \frac{kh}{R_0^2}\frac{\partial \zeta}{\partial t} \qquad \text{on } \Gamma_{w2} \times (0,T), \tag{44b}$$

where index 0 denotes reference values, ζ is a scalar representing the wall displacement in the direction of the outward unit normal vector, E is the effective Young modulus, k is the fluidity of the wall and R and h are the wall radius (in the transversal direction) and wall thickness respectively.

As a consequence of the previous choice, the resultant 1D model becomes predominantly hyperbolic in response. Thus, the canonical form of equations (43a)–(43c) along the characteristics lines is more appropriate for deriving numerical schemes [7,31]. Therefore, it will be used as the starting point in order to obtain an approximate solution in terms of the flow rate $Q = A\bar{u}$, the cross sectional area A and the pressure $\bar{p}$. Notice that this transformation only affects terms defined on the interior of the one dimensional domain, and no modifications on the boundary terms are introduced.

Correspondingly, from equation (44b) we compute the displacement ζ, from which we obtain the displacement $\boldsymbol{\gamma}_{\mathbf{Y}}$ of the ALE frame of reference by solving some well posed problem. In this work a Laplace equation is employed in order to extend the wall displacements to the interior of Ω_2. Finally, the velocity $\mathbf{w}$ of the ALE formulation is directly computed taking the time derivatives of the field $\boldsymbol{\gamma}_{\mathbf{Y}}$. Therefore, the no–slip Dirichlet boundary condition is imposed by making $\mathbf{u}_{2|\Gamma_{w2}} = \mathbf{w}_{|\Gamma_{w2}}$.

With these considerations, rewriting problem given by equations (30) and (32), eliminating the additional unknown $\bar{r}_1$ since it is known from equation (42), also considering the constitutive relations (39) and (40), and in view of equations (44) we obtain the complete formulation written in terms of the actual unknowns for this problem: *for every* $t \in (0,T)$, *find* $(Q, A, \bar{p}, \mathbf{u}_2, p_2, \boldsymbol{\gamma}_{\mathbf{Y}}) \in \mathcal{W}$ *such that*

$$\begin{aligned}
&\int_0^L \rho \left(\left.\frac{DQ}{Dt}\right|_{(-)} - f^+ \left.\frac{DA}{Dt}\right|_{(-)} - \bar{g} \right) \frac{\phi_Q}{\lambda_1} \, \mathrm{d}z \\
&\qquad + \int_0^L \rho \left(\left.\frac{DQ}{Dt}\right|_{(+)} - f^- \left.\frac{DA}{Dt}\right|_{(+)} - \bar{g} \right) \frac{\phi_Q}{\lambda_1} \, \mathrm{d}z \\
&\qquad + \int_{\Omega_2} \rho \left.\frac{\partial \mathbf{u}_2}{\partial t}\right|_{\mathbf{Y}} \cdot \mathbf{v}_2 \, \mathrm{d}\mathbf{x} + \int_{\Omega_2} \rho \nabla \mathbf{u}_2 (\mathbf{u}_2 - \mathbf{w}) \cdot \mathbf{v}_2 \, \mathrm{d}\mathbf{x} \\
&- \int_{\Omega_2} p_2 \operatorname{div} \mathbf{v}_2 \, \mathrm{d}\mathbf{x} + 2 \int_{\Omega_2} \mu \boldsymbol{\varepsilon}(\mathbf{u}_2) \cdot \boldsymbol{\varepsilon}(\mathbf{v}_2) \, \mathrm{d}\mathbf{x} - \int_{\Omega_2} \mathbf{f} \cdot \mathbf{v}_2 \, \mathrm{d}\mathbf{x} - \boxed{\int_{\Gamma_c} \bar{p} \mathbf{n}_1 \cdot \mathbf{v}_2 \, \mathrm{d}\Gamma} \\
&\qquad + \boxed{\int_{\Gamma_c} \rho (\mathbf{u}_2 \cdot \mathbf{n}_1 - \bar{u}) \frac{\phi_Q}{\lambda_3} \, \mathrm{d}\Gamma} = 0 \qquad \forall (\phi_Q, \mathbf{v}_2) \in \mathcal{W}_{\delta Q} \times W_{\delta \mathbf{u}_2},
\end{aligned} \tag{45a}$$

$$\int_0^L \rho f^+ \left(\left.\frac{DQ}{Dt}\right|_{(-)} - f^+ \left.\frac{DA}{Dt}\right|_{(-)} - \bar{g} \right) \frac{\phi_A}{\lambda_2} \, \mathrm{d}z$$
$$+ \int_0^L \rho f^- \left(\left.\frac{DQ}{Dt}\right|_{(+)} - f^- \left.\frac{DA}{Dt}\right|_{(+)} - \bar{g} \right) \frac{\phi_A}{\lambda_2} \, \mathrm{d}z + \int_{\Omega_2} \rho \operatorname{div} \mathbf{u}_2 q_2 \, \mathrm{d}\mathbf{x}$$
$$= 0 \quad \forall (\phi_A, q) \in \mathcal{W}_{\delta A} \times \mathcal{W}_{\delta p_2}, \quad (45b)$$

$$\int_{\Omega_2} \boldsymbol{\kappa} \nabla \boldsymbol{\gamma}_{\mathbf{Y}} \cdot \nabla \mathbf{v}_{\mathbf{Y}} \, \mathrm{d}\mathbf{x} = 0 \qquad \forall \mathbf{v}_{\mathbf{Y}} \in \mathcal{W}_{\delta \boldsymbol{\gamma}_{\mathbf{Y}}}, \quad (45c)$$

$$\bar{p} = \bar{p}_0 + \frac{E\pi R_0 h}{A} \left(\sqrt{\frac{A}{A_0}} - 1 \right) + \frac{k\pi R_0 h}{A} \frac{1}{2\sqrt{A_0 A}} \frac{\partial A}{\partial t} \qquad \text{in } (0, L), \quad (45d)$$
$$p_2 = p_{2_0} + \frac{Eh}{R_0^2} \zeta + \frac{kh}{R_0^2} \frac{\partial \zeta}{\partial t} \qquad \text{on } \Gamma_{w2}, \quad (45e)$$
$$\mathbf{w} = \frac{\partial \boldsymbol{\gamma}_{\mathbf{Y}}}{\partial t} \qquad \text{in } \Omega_2. \quad (45f)$$

Here we have that $\boldsymbol{\gamma}_{\mathbf{Y}} = \zeta \mathbf{n}_2$ on Γ_{w2}, and since $\mathbf{w} = \mathbf{u}_{2|\Gamma_{w2}}$ on Γ_{w2}, it is $\mathbf{u}_{2|\Gamma_{w2}} = \frac{\partial \boldsymbol{\gamma}_{\mathbf{Y}}}{\partial t}_{|\Gamma_{w2}}$. In this way, the admissible variations of $\mathbf{u}_2$ are such that $\mathbf{v}_{2|\Gamma_{w2}} = 0$. Also ϕ_Q and ϕ_A are the corresponding test functions of the flow rate equation and of the area equation in the 1D model. In expressions (45a) and (45b) quantities $\frac{D(\cdot)}{Dt}|_{(\pm)}$ denote total time derivatives with respect to the characteristics lines corresponding to celerities $f^{\pm} = \frac{Q}{A} \pm c$, being $c = \sqrt{\frac{A}{\rho} \frac{\partial \bar{p}}{\partial A}}$ the speed of sound into the vessel, and function $\bar{g}$ is given by $\bar{g} = f^z - \frac{8\pi\mu}{A} Q$. Also λ_i, $i = 1, 2, 3$, are constants such that these equations are dimensionally consistent. In equation (45c), $\boldsymbol{\kappa}$ is a kind of diffusivity tensor that may be set conveniently. In this work the simplest case is used, being $\boldsymbol{\kappa}$ the identity tensor. Finally, essential boundary conditions are given in function set $\mathcal{W}$.

5.3 Time discretization and finite element approximation

In this section we describe the numerical techniques used in approximating formulation (45). Since these techniques are well known, we limit ourselves to mentioning, when necessary, the corresponding references and no further details are given. Thus we can summarize the approximation process as follows:

- The variational formulation is discretized first in time by means of a single step finite difference method corresponding to a classical θ–scheme for both 1D and 3D parts.
- For variables Q, A, $\bar{p}$ of the 1D model $\mathbb{P}_1$ finite elements are used, while for variables $\mathbf{u}_2$, p_2 of the 3D model $\mathbb{P}_1^B - \mathbb{P}_1$ finite elements are considered, where supra index B indicates the use of bubble functions for the velocity field

[2]. Degrees of freedom $\boldsymbol{\gamma}_{\mathbf{Y}}$ are also approximated with $\mathbb{P}_1$ finite elements, and finally the velocity of the frame of reference $\mathbf{w}$ is computed from the displacements $\boldsymbol{\gamma}_{\mathbf{Y}}$ by a backward Euler difference.

- For both 1D and 3D parts, stabilization terms must be included with the aim of avoiding the well known non–physical oscillating solutions present when using a Galerkin approximation. For the 1D model these terms are incorporated along the characteristics lines and correspond to a Galerkin Least Squares formulation [20,37]. For the 3D model the stabilization terms correspond to the Streamline Upwind Petrov Galerkin technique with a suitable stabilization parameter [19].
- Finally, the nonlinearities of the problem are treated in all cases with Picard iterations.

5.4 The monolithic and segregated coupling schemes

The complete set of discrete equations is then obtained following the guidelines exposed in the previous section. Here we present the resulting linearized algebraic form with the aim of highlighting how coupling terms appear within the monolithic scheme. Thus the discretized problem reads as follows: *for each time step t_{n+1}, $n = 0, 1, 2, \ldots, N$, until a convergence criterion is achieved perform iterations $k = 1, 2, \ldots$, solving the following system of linear equations*

$$\begin{pmatrix} \mathbf{A}^k_{QQ} & 0 & \mathbf{A}^k_{Q\bar{p}} & \mathbf{A}^k_{Q\mathbf{u}_2} & 0 & 0 \\ 0 & \mathbf{A}^k_{AA} & \mathbf{A}^k_{A\bar{p}} & 0 & 0 & 0 \\ \mathbf{A}^k_{\bar{p}Q} & 0 & \mathbf{A}^k_{\bar{p}\bar{p}} & 0 & 0 & 0 \\ 0 & 0 & \mathbf{A}^k_{\mathbf{u}_2\bar{p}} & \mathbf{A}^k_{\mathbf{u}_2\mathbf{u}_2} & \mathbf{A}^k_{\mathbf{u}_2 p_2} & \mathbf{A}^k_{\mathbf{u}_2\boldsymbol{\gamma}_{\mathbf{Y}}} \\ 0 & 0 & 0 & \mathbf{A}^k_{p_2\mathbf{u}_2} & 0 & 0 \\ 0 & 0 & 0 & 0 & \mathbf{A}^k_{\boldsymbol{\gamma}_{\mathbf{Y}} p_2} & \mathbf{A}^k_{\boldsymbol{\gamma}_{\mathbf{Y}}\boldsymbol{\gamma}_{\mathbf{Y}}} \end{pmatrix} \begin{pmatrix} \mathbf{U}^{k+1}_Q|_{n+1} \\ \mathbf{U}^{k+1}_A|_{n+1} \\ \mathbf{U}^{k+1}_{\bar{p}}|_{n+1} \\ \mathbf{U}^{k+1}_{\mathbf{u}_2}|_{n+1} \\ \mathbf{U}^{k+1}_{p_2}|_{n+1} \\ \mathbf{U}^{k+1}_{\boldsymbol{\gamma}_{\mathbf{Y}}}|_{n+1} \end{pmatrix} = \begin{pmatrix} \mathbf{f}^k_Q \\ \mathbf{f}^k_A \\ \mathbf{f}^k_{\bar{p}} \\ \mathbf{f}^k_{\mathbf{u}_2} \\ \mathbf{f}^k_{p_2} \\ \mathbf{f}^k_{\boldsymbol{\gamma}_{\mathbf{Y}}} \end{pmatrix}. \tag{46}$$

Here, at time t_{n+1} and for unknowns X, Y, $\mathbf{A}^k_{XY}$ denote the corresponding block computed in the iteration k, $\mathbf{U}^{k+1}_X|_{n+1}$ the nodal degrees of freedom in the iteration $k+1$ and $\mathbf{f}^k_X$ the forcing terms in the iteration k.

In the system of linear equations (46) blocks $\mathbf{A}^k_{Q\mathbf{u}_2}$ and $\mathbf{A}^k_{\mathbf{u}_2\bar{p}}$ represent the algebraic counterpart of the coupling terms between both 1D and 3D models boxed in expressions (45). In particular, these matrixes comprise the coupling relation between the degrees of freedom of the 1D node located at $z = L$ and the 3D nodes that lie on boundary Γ_c.

The algebraic form (46) was used for computations in all the examples presented in this work unless the contrary is explicitly stated, and was solved

using a Preconditioned Conjugated Gradient Square method [32]. The result is a robust numerical scheme that efficiently manages the coupling of multidimensional models.

Alternatively, a decoupled numerical scheme may be devised in case of working with validated stand–alone 1D and 3D FEM codes. In this case we can split the computations by performing iterations between the 1D and 3D subproblems. In this situation the segregated counterpart of system (46) would read as follows: *for each time step* t_{n+1}*,* $n = 0, 1, \ldots, N$*, until a convergence criterion is achieved perform iterations* $k = 0, 1, \ldots$*, solving*

$$\begin{array}{lll} \text{i.} & \mathbf{A}^k_{1\mathrm{D}}\mathbf{U}^{k+1}_{1\mathrm{D}}|_{n+1} = \mathbf{f}^{k,\omega}_{1\mathrm{D}} & \text{1D problem,} \\ \text{ii.} & \mathbf{A}^k_{3\mathrm{D}}\mathbf{U}^{k+1}_{3\mathrm{D}}|_{n+1} = \mathbf{f}^{k,\omega}_{3\mathrm{D}} & \text{3D problem,} \end{array}$$

where indexes 1D and 3D correspond to the subblocks of the 1D and 3D problem respectively, in particular we have

$$\mathbf{f}^{k,\omega}_{1\mathrm{D}} = \begin{pmatrix} \widetilde{\mathbf{f}}^{k,\omega}_Q \\ \mathbf{f}^k_A \\ \mathbf{f}^k_{\bar{p}} \end{pmatrix} \qquad \mathbf{f}^{k,\omega}_{3\mathrm{D}} = \begin{pmatrix} \widetilde{\mathbf{f}}^{k,\omega}_{\mathbf{u}_2} \\ \mathbf{f}^k_{p_2} \\ \mathbf{f}^k_{\gamma_\mathbf{Y}} \end{pmatrix}, \tag{47}$$

and where

$$\begin{aligned} \widetilde{\mathbf{f}}^{k,\omega}_Q &= \mathbf{f}^k_Q - \Big[\omega \mathbf{A}^k_{Q\mathbf{u}_2}\mathbf{U}^k_{\mathbf{u}_2}|_{n+1} + (1-\omega)\mathbf{A}^k_{Q\mathbf{u}_2}\mathbf{U}^{k-1}_{\mathbf{u}_2}|_{n+1}\Big], \\ \widetilde{\mathbf{f}}^{k,\omega}_{\mathbf{u}_2} &= \mathbf{f}^k_{\mathbf{u}_2} - \Big[\omega \mathbf{A}^k_{\mathbf{u}_2\bar{p}}\mathbf{U}^{k+1}_{\bar{p}}|_{n+1} + (1-\omega)\mathbf{A}^k_{\mathbf{u}_2\bar{p}}\mathbf{U}^k_{\bar{p}}|_{n+1}\Big], \end{aligned} \tag{48}$$

being $0 < \omega \leq 1$ a subrelaxation parameter that acts between subdomain iterations. The decoupling scheme presented here corresponds to a Gauss-Seidel decomposition, and the well–posedness of both problems is accounted for by contributions in forcing terms $\widetilde{\mathbf{f}}^{k,\omega}_Q$ and $\widetilde{\mathbf{f}}^{k,\omega}_{\mathbf{u}_2}$.

6 Numerical assessments

In this section several situations are considered. The first example illustrates the case for which we have a fairly short–wavelength wave propagating along a pipe simulated by using 3D and 1D models. Here we encounter a non–physical response of the model due to the appearance of spurious reflections. The next two examples are related to the direct application of the formulation developed to the cardiovascular modelling. In particular, the second one exemplifies all the potentialities of using this kind of model, being a clear situation for which other ways of imposing boundary conditions are rather cumbersome to implement. Other examples in this direction can be found in [4,25].

In all these examples we use 3D geometries embedded in a 1D model for which we have two or even three coupling interfaces. Consequently, we perform comparisons at nodes placed at coupling interfaces for two situations: when solving with just the pure 1D model and when using the 3D–1D formulation proposed in this work. The monolithic scheme is used in all the examples. Nevertheless, a first study of the performance of the segregated scheme is included in the second part of section 6.2.1.

The nomenclature used in describing the 3D geometry and properties in the examples is the following

L : length of the vessel,	R : radius of the vessel,
h : thickness of the arterial wall,	E : Young modulus of the arterial wall,
k : fluidity of the arterial wall,	C : speed of sound into the vessel,
p_0 : reference pressure.	

6.1 Case 1: Wave travelling along a dimensionally heterogeneous domain

This first example has the purpose of presenting a simple situation for which we put in evidence the effective coupling between models of different dimensionality. Another goal of this example is to analyze possible artificial phenomena appearing at the coupling interfaces as a result of the dimensional heterogeneity of the model. In this way we focus the analysis in the quantities defined on the 1D model.

We use the configuration shown in Figure 4, where we have an entrance represented by a pipe considered as a 1D model and an exit modelled in the same way, whereas a 3D model is used connecting those regions. We set a pressure boundary condition at the entrance by a curve of the form $p(t) = p_{\max} \sin^2\left(\frac{\pi t}{t_F}\right)$, with $p_{\max} = 10000$ dyn/cm^2 and $t_F = 0.005$ sec for $0 \leq t \leq t_F$, and $p(t) = 0$ for $t > t_F$. This curve is also shown in Figure 4. All the geometrical and mechanical properties are equal for both models so as to keep the consistency of the whole model. Being L_T the total length and L_{3D} just the corresponding one to the 3D model, it is $L_T = 25$ cm, $L_{3D} = 5$ cm, $R = 0.5$ cm, $h = 0.05$ cm, $E = 20.0 \cdot 10^6$ dyn/cm^2, k is null, $C = 1000$ cm/sec, p_0 is null, $\rho = 1.0$ g/cm^3 and $\mu = 0.4$ poise. The Reynolds number reaches values around $\mathrm{Re} = 12$ in the peak of the wave. The number of nodes and degrees of freedom for this case is about 41100 and 283400 respectively, while the time step used is about $\Delta t = 2.5 \cdot 10^{-5}$ sec within a total run time $T = 2.5 \cdot 10^{-2}$ sec.

In this case we also consider a special situation that simulates the absence of viscosity. For the 1D model we set $\mu = 0$, while for the 3D model we assume a total slip condition in the axial direction over the boundary Γ_{w2}, but we keep

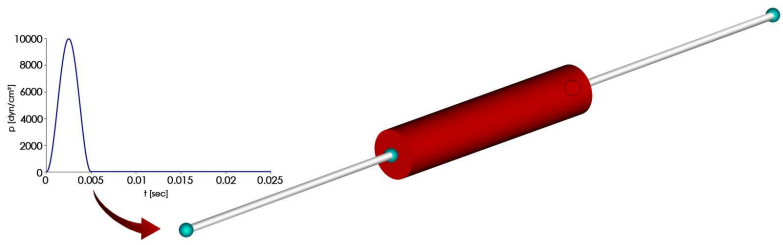

Fig. 4. Cylindrical geometry for case 1 formed by 3D and 1D parts.

the value of the viscosity equal to 0.4 poise.

In figure 5 the flow rate and pressure at the entrance of the 3D region are shown, comparing the results of the pure 1D model and the corresponding to the 3D–1D coupled model. In this figure it is possible to appreciate the reflected flow rate wave whose amplitude reaches 1.9% of the inflowing flow wave in the pure 1D model.

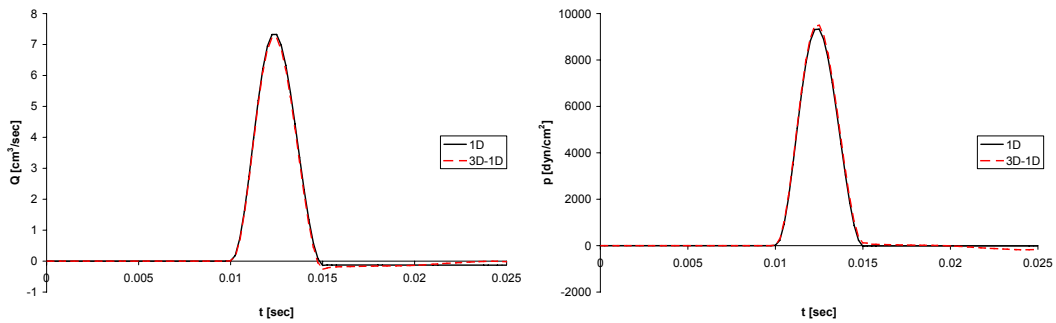

(a) Evolution of the flow rate. (b) Evolution of the pressure.

Fig. 5. Results at the entrance of the 3D region on the coupling interface.

The sequence of Figures 6 shows the pressure wave (its mean value inside the 3D region) computed with formulation (45) travelling along the 1D–3D–1D domain. The appearance of spurious reflections travelling in the opposite direction when the wave is passing through both coupling interfaces can be clearly appreciated (see Figures 6(b)–6(d)). The amplitude of the reflected wave is about 2% of the amplitude of the inflowing wave corresponding to the pure 1D model at the same location. This phenomenon can also be noticed in the examples presented in [11,12] (see figures 7 and in pages 580 and 398 respectively) with a reflected wave amplitude apparently larger. It is also worth mentioning that in the present work no numerical techniques for avoiding these reflections were used. When using the total slip condition over the wall in the 3D domain we observe, according to Figures 7, almost no spurious reflections, that is, the coupling interface is transparent regarding the waves travelling along the mixed domain. The analysis of the results obtained with these examples indicates that the following dimensionless numbers $\frac{1}{\mathrm{Re}}\frac{D}{\lambda}$ and $\frac{1}{\mathrm{Re}}$, where Re is the Reynolds number, D is the diameter of the pipe and λ the wavelength, may be considered as indicators of the presence of spurious

reflections. This issue will be further discussed in Section 6.3. For the examples presented in the following the value of these indexes ensures the almost absence of spurious reflections.

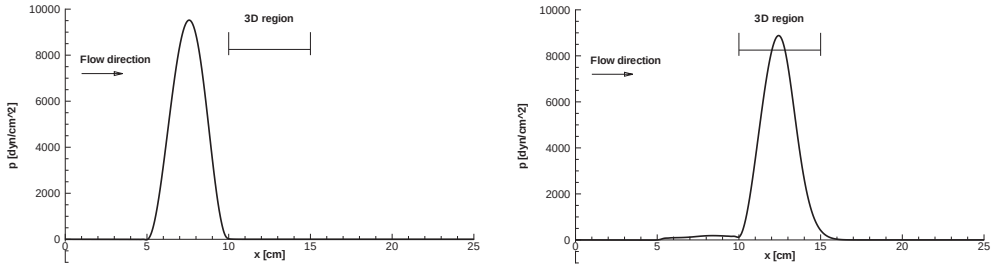

(a) $t = 0.01$ sec.

(b) $t = 0.015$ sec.

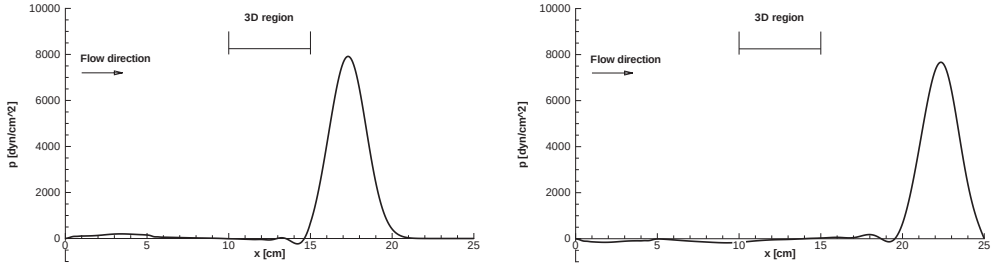

(c) $t = 0.020$ sec.

(d) $t = 0.025$ sec.

Fig. 6. Results for computations with the derived formulation.

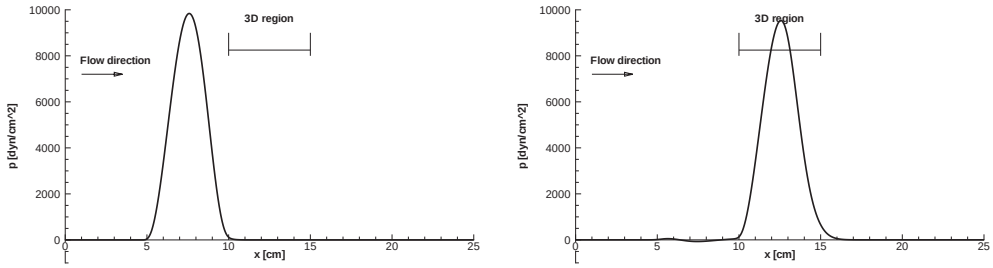

(a) $t = 0.01$ sec.

(b) $t = 0.015$ sec.

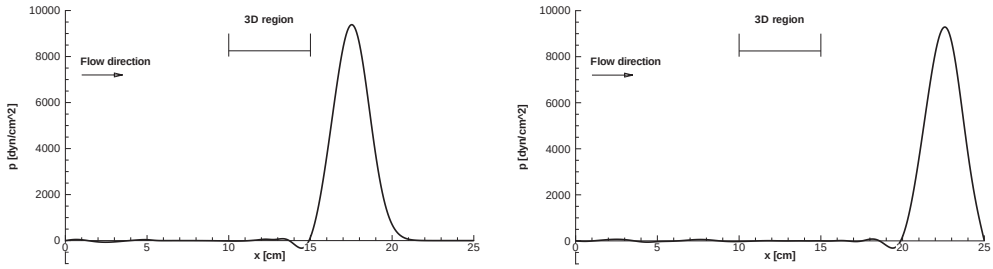

(c) $t = 0.020$ sec.

(d) $t = 0.025$ sec.

Fig. 7. Results for computations in the simulated absence of viscosity.

6.2 Case 2: Applications in cardiovascular modelling

In the applications to hemodynamics the model representing the whole cardiovascular system, with all geometrical and mechanical parameters, was taken from [3] and is shown in Figure 8(a). The 3D geometries were geometrically and mechanically adapted to the values of the corresponding segments replaced in the 1D arterial tree. The system is fed with two flow rate curves at the aortic root taken from [33,34] and shown in Figure 8(b). Peripheral beds are modelled by Windkessel lumped models.

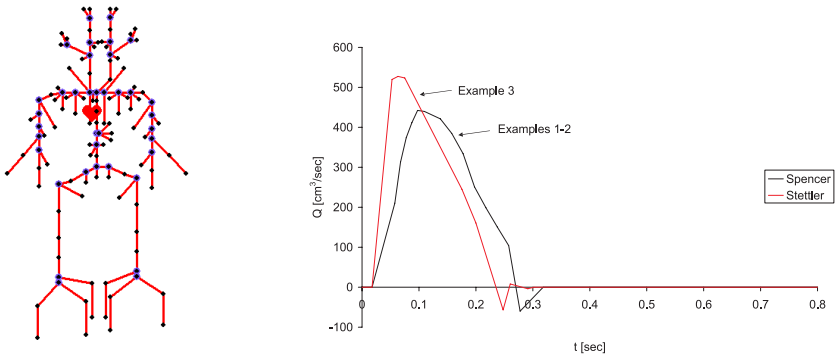

(a) 1D arterial tree. (b) Flow rate curves at the aortic root.

Fig. 8. Arterial tree and the corresponding boundary condition at the aortic root.

It was taken density $\rho = 1.04$ g/cm^3 and viscosity $\mu = 0.04$ poise, while in all cases the time step used is about $\Delta t = 1.25 \cdot 10^{-3}$ sec for a heart beat of $T = 0.8$ sec. In all cases three cardiac beats were simulated starting from the at rest state. The results presented in the following sections correspond to the third beat. It is interesting to mention that no differences, concerning the behavior of the 3D–1D coupled model and the comparisons with the pure 1D model, were observed in the process before the system reaches the periodic state.

6.2.1 Example 1: Blood flow in the abdominal aorta artery

For this example the situation is shown in Figure 9 and the heart ejection curve used is shown in Figure 8(b). We have replaced a segment of the abdominal aorta artery of the 1D arterial tree with a 3D cylindrical geometry. In this example we have $L = 5.7$ cm, $R = 0.57$ cm, $h = 0.08$ cm, $E = 4.0 \cdot 10^6$ dyn/cm^2, $k = 4.44 \cdot 10^4$ dyn sec/cm^2, $C = 519.5$ cm/sec and $p_0 = 1.0 \cdot 10^5$ dyn/cm^2. The Reynolds number reaches values around Re $= 1700$ in the peak of the systole. The number of nodes and degrees of freedom for this case is about 41300 and 285200 respectively.

Figures 10 show the flow rate Q and the pressure $\bar{p}$ at both coupling interfaces

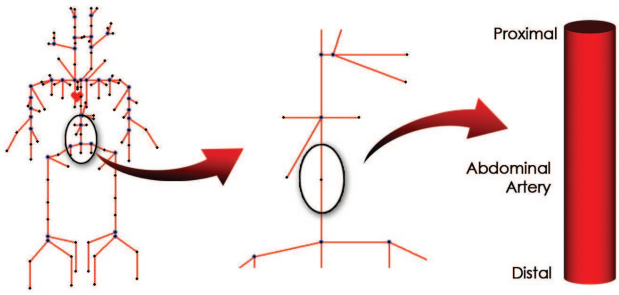

Fig. 9. 3D segment of the abdominal aorta artery embedded in a 1D arterial tree.

named Γ_p and Γ_d indicating proximal and distal locations respectively. In these figures the results given by formulation (45) together with the pure 1D model are presented. It is observed a good agreement with the results of the pure 1D model, evidencing the suitability of the formulation devised in the present work.

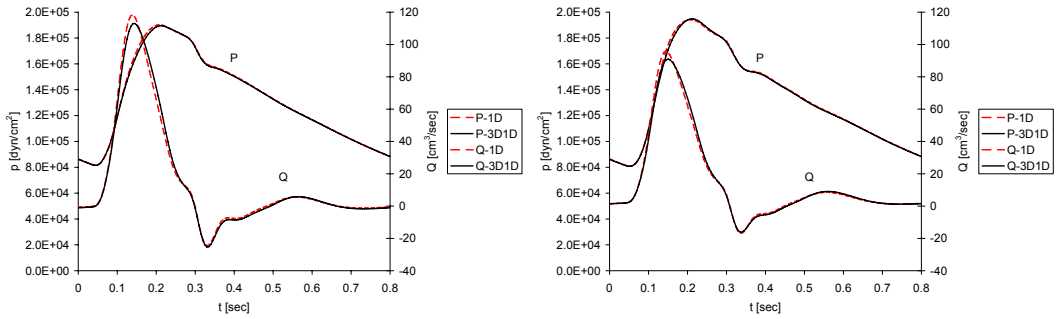

(a) Curves at Γ_p. (b) Curves at Γ_d.

Fig. 10. Flow rate and pressure curves at coupling interfaces Γ_p and Γ_d.

For this case the monolithic and segregated coupling schemes presented in section 5.4 are also compared. A third interesting situation is considered by using the linearized version of the segregated scheme, that is, advancing in time computing the 3D problem and then the 1D problem without iterating between them. For the iterative version of the segregated scheme different values of ω are tested with the aim of studying the convergence properties.

Table 1 summarizes the study of the convergence properties of the iterative scheme, showing the maximum number of iterations performed for each of the tested values of ω. The time step needed to be reduced when the iterative solver did not converge. For this reason different time steps are shown in the same table. The configuration of the solver is fixed for all cases. It can be seen that the best choice for ω, at least for regimes similar to those found in cardiovascular modelling, is around 0.8.

Figure 11 shows the flow rate Q and the pressure $\bar{p}$ at the coupling interface Γ_p just for three cases for the sake of clarity. The curve *Coupled* corresponds to the 3D–1D monolithic scheme, *Seg Linear* denotes the linearized version

Case	Maximum number of iterations	Minimum time step needed [sec]
$\omega = 1.0$	13	$3.125 \cdot 10^{-4}$
$\omega = 0.8$	5	$6.25 \cdot 10^{-4}$
$\omega = 0.6$	9	$6.25 \cdot 10^{-4}$
$\omega = 0.4$	12	$6.25 \cdot 10^{-4}$
$\omega = 0.2$	25	$3.125 \cdot 10^{-4}$

Table 1
Convergence details and time steps needed for the different cases.

of the segregated scheme and *Seg* $\omega = 0.8$ is the segregated scheme with subrelaxation parameter equal to 0.8. Observe that no differences appear in the situation studied. This result shows an interesting aspect held by the *Seg Linear* case at least for the regimes seen in the abdominal aorta artery, and that is the possibility of solving both problems, the 3D and the 1D, separately. This situation is the more convenient from the computational cost point of view.

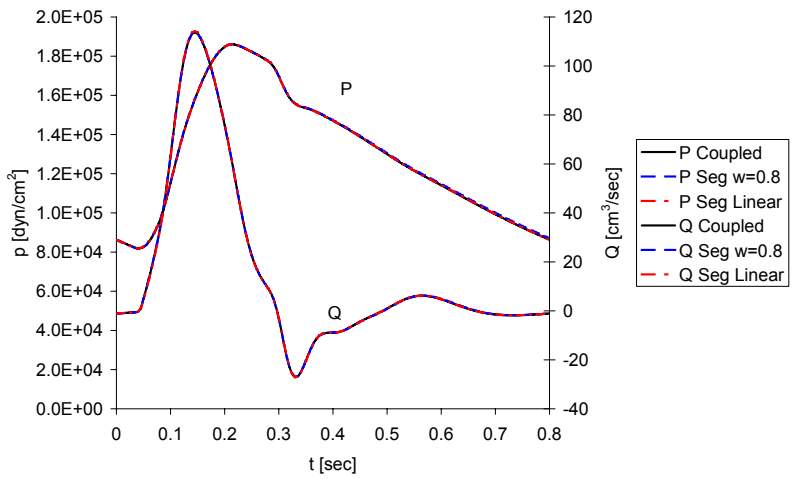

Fig. 11. Flow rate at Γ_p for the different coupling schemes.

6.2.2 Example 2: Blood flow in a stenosed carotid artery bifurcation

In this situation we have the configuration shown in Figure 12 and the heart ejection curve used is also shown in Figure 8(b). We have replaced the district corresponding to the carotid bifurcation of the 1D arterial tree with a 3D standard carotid bifurcation geometry. The goal of this example is to analyze how mean quantities (flow rate and pressure) are perturbed at the coupling interfaces, or even at any location of the 1D model of the arterial tree, when an obstacle such as a simulated stenosis is introduced by strangling the carotid sinus in the 3D district. We denote N the normal situation, $S80$ a situation with a stenosis of 80% and $S95$ a situation with a stenosis of 95%. These

percentages represent the reduction of the area at the $SS3$ section (see Figure 13). This kind of analysis cannot be performed unless we use this kind of formulations since only here the systemic response of the complete model is properly accounted for. Indeed, assume that we have acquired measurements from a patient in order to set the boundary conditions for the 3D problem. Such measurements remain valid only for the conditions in which they were obtained (for example for a given geometry). Then, introducing geometrical perturbations in the actual domain, for instance a stenosis, makes these boundary conditions invalid since such conditions depends on the systemic response of the arterial network to changes in the geometry of the vascular district.

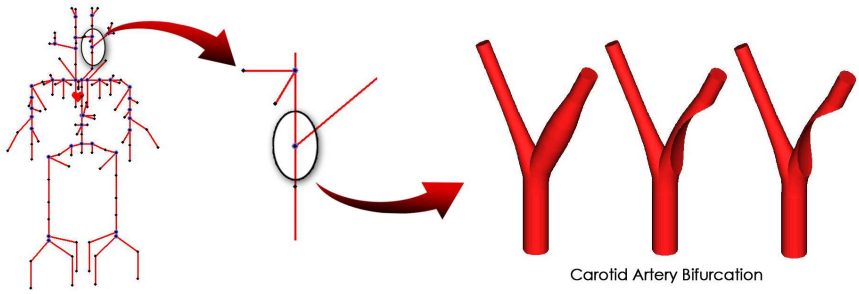

Fig. 12. 3D carotid artery bifurcation embedded in a 1D arterial tree.

Indexes c, e and i refer to common, external and internal segments. In this example we have $h = 0.1R$, $E_c = 4.0 \cdot 10^6$ dyn/cm^2, $E_e = E_i = 8.0 \cdot 10^6$ dyn/cm^2, $k_c = 4.44 \cdot 10^4$ dyn sec/cm^2, $k_e = k_i = 8.88 \cdot 10^4$ dyn sec/cm^2, $C = 439$ cm/sec and $p_0 = 8.0 \cdot 10^4$ dyn/cm^2. A detailed description of the geometry is given in Figure 13 and in Table 2.

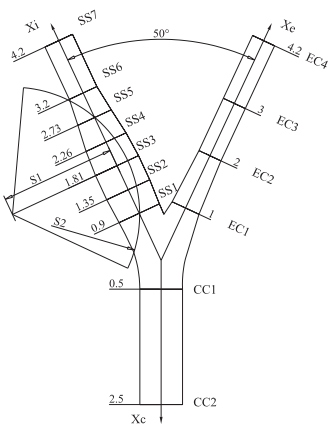

Section	Diameter [cm]	
CC1	0.74	
CC2	0.74	
SS1	0.77182	
SS2	0.8214	
SS3	0.8214	
SS4	0.76368	
SS5	0.6364	
SS6	0.5254	
SS7	0.5254	
EC1	0.51356	
EC2	0.42032	
EC3	0.42032	
EC4	0.42032	
(stenosis)	80%	95%
S1	2	1.5
S2	2.20535	1.835

Fig. 13. Geometry and stenosis morphology.

Table 2. Geometric parameters.

The Reynolds number reaches values around Re = 640 for the N case, Re = 720 for the $S80$ case and Re = 760 for the $S95$ case, always in the peak of the systole and at the section SS3 in the carotid sinus. The number of nodes and

degrees of freedom for this case is about 69200 and 480500 for the case $S95$, 40400 and 279000 for the case $S80$ and 55800 and 386900 for the case N.

Figures 14(a), 14(b) and 14(c) show how the mean quantities at coupling interfaces are affected due to the presence of the stenosis. The results correspond to the coupled model. It can be observed that the arterial pulse does not suffer significant perturbations in the case $S80$. Only in the extreme case $S95$ appreciable variations of the pressure and flow rate curves are noticeable, especially at the exit of the internal carotid artery. The mean flow supplied through the internal carotid suffers a reduction of 9% with respect to the normal condition. To understand the results it must be pointed out that no vasodilation was considered here, although nothing impedes to incorporate this phenomenon in order to improve the simulation. In this sense the percentage of reduction of the flow rate in a cardiac cycle could change significantly when considering the aforementioned adaptive process of vasodilation.

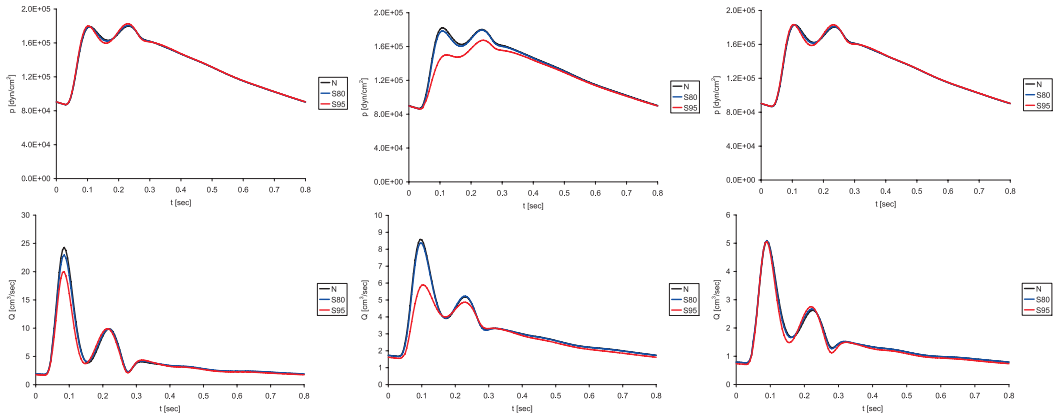

(a) Common carotid. (b) Internal carotid. (c) External carotid.

Fig. 14. Comparison of the results for the levels of stenosis considered.

6.3 Final remarks

This section is devoted to the discussion of the condition (43e). Certainly, along the derivation of the 1D model some terms associated to viscous effects were neglected. As a result, we obtained the Euler equation at Γ_c given by (43e). Therefore, it is observed that the continuity of pressure is given for two situations: (i) non–viscous flows and (ii) long wavelengths and/or large Reynolds numbers. The second situation was exemplified in Subsection 6.2, whereas the first case was considered in the results shown in the sequence of Figures 7 of the case presented in Subsection 6.1. Here, the absence of viscosity entails the significant reduction of spurious reflections.

As pointed out previously, it is important to characterize when spurious reflections are likely to appear. In this way we perform a dimensionless analysis of

the coupling condition related to the normal traction continuity. If we measure the pressure in terms of twice the kinetic energy, ρU^2, being U a representative velocity, and if we take the wavelength λ as a representative length for the normal derivatives and the diameter of the pipe D as the representative length for the tangential derivatives, the dimensionless counterpart of equation (43e) can be split into two parts as follows

$$\begin{aligned} -p^* &= -p_2^* + \frac{1}{\mathrm{Re}}\frac{D}{\lambda}\boldsymbol{\varepsilon}^*(\mathbf{u}_2^*)\mathbf{n}_1 \cdot \mathbf{n}_1, \\ 0 &= \frac{1}{\mathrm{Re}}\boldsymbol{\varepsilon}^*(\mathbf{u}_2^*)\mathbf{n}_1 \cdot \mathbf{t}_1 \end{aligned} \tag{49}$$

where $\mathrm{Re} = \frac{\rho U D}{\mu}$ is the Reynolds number, $(\cdot)^*$ denotes a non–dimensional quantity and $\mathbf{t}_1$ is an unit vector on the plane corresponding to the interface Γ_c such that it is perpendicular to $\mathbf{n}_1$. Hence, the dimensionless numbers $\frac{1}{\mathrm{Re}}\frac{D}{\lambda}$ and $\frac{1}{\mathrm{Re}}$ may be associated to the presence or not of spurious reflections. In examples 1 and 2, with application in the simulation of the cardiovascular system (see Subsection 6.2), we observe that the smallness of these numbers allows us to say that we have almost no spurious reflections. This can be seen in the range of values shown in Table 3. In building this table we have used $\lambda = 5$ cm for the situation of Subsection 6.1 and $\lambda = 500$ cm for the situation of Subsection 6.2. Consequently, the smallness of the dimensionless numbers $\frac{1}{\mathrm{Re}}\frac{D}{\lambda}$ and $\frac{1}{\mathrm{Re}}$ may be used in order to indicate when the model can be considered accurate in the sense of the spurious reflections generated by the coupling interfaces.

	Case 1	Case 2 Example 1	Case 2 Example 2
$\frac{1}{\mathrm{Re}}\frac{D}{\lambda}$	$4.17 \cdot 10^{-2}$	$1.34 \cdot 10^{-6}$	$2.96 \cdot 10^{-6}$
$\frac{1}{\mathrm{Re}}$	$2.09 \cdot 10^{-1}$	$5.88 \cdot 10^{-4}$	$2.00 \cdot 10^{-3}$

Table 3
Values of $\frac{1}{\mathrm{Re}}\frac{D}{\lambda}$ and $\frac{1}{\mathrm{Re}}$ for the examples presented in Subsections 6.1 and 6.2.

However, since there exists several other aspects that must be integrated in the analysis of this problem, the previous explanation must be considered as the starting point for further investigation on this matter.

7 Conclusions

In this work we have proposed a variational principle that manages possible discontinuities that arise when different underlying kinematics are considered on some partition of a given domain. Consequently, this framework resulted in a suitable and unified strategy that efficiently tackles the problem of coupling

models of different dimensionality. For usual situations encountered in cardiovascular modelling we have obtained good results for the simultaneous use of 3D and 1D models, showing the capabilities of the formulation to handle the coupling conditions in a natural way. Also, the corresponding monolithic and the segregated coupling schemes were numerically compared, and for the regimes established in the arterial tree both schemes presented identical results. From the numerical examples it is possible to see that the spurious reflections present for short wavelength waves are significantly reduced for the non–viscous case. Hence, we conclude that the role of the viscous shear stress must be a subject of further investigation.

Acknowledgements

Pablo Javier Blanco (140686/2005–3) was supported by the Brazilian agency CNPq. The support of this agency is gratefully acknowledged. The authors would also like to acknowledge the reviewers for their valuable comments and constructive suggestions that helped to improve the quality of the manuscript.

References

[1] M. Anliker, R.L. Rockwell and E. Ogden, Nonlinear analysis of flow pulses and shockwaves in arteries. Part I: derivations and properties of mathematical model, ZAMP 22 (1971) 217–246.

[2] D.N. Arnold, F. Brezzi and M. Fortin, A stable finite element for the Stokes equations, Calcolo 21 (1984) 337–344.

[3] A.P. Avolio, Multi–branched model of the human arterial system, Med. Biol. Engrg. Comp. 18 (1980) 709–718.

[4] P.J. Blanco, I. Larrabide, S.A. Urquiza and R.A. Feijóo, Sensitivity of blood flow patterns to the constitutive law of the fluid, in: Proc. ECCM2006 - III European Conference on Computational Mechanics Solids, Structures and Coupled Problems in Engineering, C.A. Mota Soares et al. (Eds.), Lisbon, Portugal, June 2006.

[5] F. Brezzi and M. Fortin, Mixed and Hybrid Finite Element Methods, (Springer–Verlag, New York, 1991).

[6] C.G. Caro, J.M. Fitz–Gerald, R.C. Schroter, Atheroma and arterial wall shear dependent mass transfer mechanism for atherogenesis, Proc. Royal Society of London, Biology B177 (1971) 109–159.

[7] R. Courant, D. Hilbert, Methods of Mathematical Physics, Vol. II, (Interscience Publishers, New York, 1962).

[8] A. Ern, J.L. Guermond, Theory and Practice of Finite Elements (Springer–Verlag, New York, 2004).

[9] R.A. Feijóo, L. Bevilacqua, L. Rojas, A variational principle for the Laplace's operator with applications in the torsion of composite rods, Int. J. Sol. Struct. 10 (1974) 1091–1102.

[10] L. Formaggia, F. Nobile, A. Quarteroni and A. Veneziani, Multiscale modelling of the vascular system: a preliminary analysis, Comp. Vis. Science 2 (1999) 75–83.

[11] L. Formaggia, J.F. Gerbeau, F. Nobile and A. Quarteroni, On the coupling of 3D and 1D Navier–Stokes equations for flow problems in compliant vessels, Comp. Meth. Appl. Mech. Engrg. 191 (2001) 561–582.

[12] L. Formaggia, J.F. Gerbeau, F. Nobile and A. Quarteroni, Numerical treatment of defective boundary conditions for the Navier–Stokes equations, SIAM J. Numer. Anal. 40 (2002) 376–401.

[13] D.P. Giddens, C.K. Zarins, S. Glagov, The role of fluid mechanics in the localization and detection of atherosclerosis, J. Biomech. Engrg. 115 (1993) 588–594.

[14] V. Girault and P.-A. Raviart, Finite Element Methods for Navier–Stokes Equations. Theory and Algorithms, (Springer–Verlag, Berlin, 1986).

[15] J.G. Heywood, R. Rannacher and S. Turek, Artificial boundaries and flux and pressure conditions for the incompressible NavierStokes equations, Int. J. Num. Meth. Fluids 22 (1996) 325–352.

[16] R. Holenstein, P. Niederer and M. Anliker, A viscoelastic model for use in predicting arterial pulse waves, J. Biomech. Engrg. 102 (1980) 318–325.

[17] T.J.R. Hughes and J. Lubliner, On the one–dimensional theory of blood flow in the larger vessels, Math. Biosciences 18 (1973) 161–170.

[18] T.J.R. Hughes, W.K. Liu, T.K. Zimmermann, Lagrangian–Eulerian finite element formulation for incompressible viscous flows, Comp. Meth. Appl. Mech. Engrg. 29 (1981) 329–349.

[19] T.J.R. Hughes, L.P. Franca and M. Mallet, A new finite element formulation for computational fluid dynamics: VI. Convergence analysis of the generalized SUPG formulation for linear time–dependent multidimensional advective–diffusive systems, Comp. Meth. Appl. Mech. Engrg. 63 (1987) 97–112.

[20] T.J.R. Hughes, L.P. Franca and G.M. Hulbert, A new finite element formulation for computational fluid dynamics: VIII. The Galerkin/least squares method for advective–diffusive equations, Comp. Meth. Appl. Mech. Engrg. 73 (1989) 173–189.

[21] Y. Kivity and R. Collins, Nonlinear fluid–shell interactions: application to blood flow in large arteries, Int. Sym. Discrete Meth. Engrg. (1974) 476–488.

[22] Y. Kivity and R. Collins, Nonlinear wave propagation in viscoelastic tubes: application to aortic rupture, J. Biomech. 7 (1974) 67–76.

[23] D.N. Ku, D.P. Giddens, C.K. Zarins, S. Glagov, Pulsatile flow and atherosclerosis in the human carotid bifurcation, Arteriosclerosis 5 (1985) 293–302.

[24] K. Lagana, G. Dubini, F. Migliavacca, R. Pietrabissa, G. Pennati, A. Veneziani and A. Quarteroni, Multiscale modelling as a tool to prescribe realistic boundary conditions for the study of surgical procedures, Biorheology 39 (34) (2002) 359-364.

[25] I. Larrabide, P.J. Blanco, S.A. Urquiza and R.A. Feijóo, Sensitivity of blood flow in stenosed carotid bifurcation, in: Proc. ICCB2005 - II International Conference on Computational Bioengineering, H. Rodrigues et al. (Eds.), Lisbon, Portugal, September 2005.

[26] R. Löhner, J. Cebral, O. Soto, P. Yim and J.E. Burgess, Applications of patient–specific CFD in medicine and life sciences, Int. J. Num. Meth. Fluids 43 (2003) 637–650.

[27] P.F. Niederer, Damping mechanisms and shock–like transitions in human arterial tree, ZAMP 36 (1985) 204–220.

[28] M. Oshima, R. Torii, T. Kobayashi, N. Taniguchi and K. Takagi, Finite element simulation of blood flow in the cerebral artery, Comp. Meth. Appl. Mech. Engrg. 191 (2001) 661–671.

[29] K. Perktold and G. Rappitsch, Computer simulation of local blood flow and vessel mechanics in a compliant carotid artery bifurcation model, J. Biomech. 28 (1995) 845–856.

[30] A. Quarteroni, M. Tuveri and A. Veneziani, Computational vascular fluid dynamics: problems, models and methods, Comp. Vis. Science 2 (2000) 163–197.

[31] R.D. Rychtmyer and K.W. Morton, Difference Methods for Initial–Value Problems, (Interscience Publishers, New York, 1967).

[32] Y. Saad, SPARSEKIT: a basic tool kit for sparse matrix computation version 2, http//:www.users.cs.umn.edu/˜saad/software/SPARSEKIT/sparsekit.html, University of Illinois (1985).

[33] M.P. Spencer and A.B. Deninson, The square–wave electro–magnetic flowmeter. Theory of operation and design of magnetic probes for clinical and experimental applications, I.R.E. Trans. Med. Elect. 6 (1959) 220–228.

[34] J.C. Stettler, P. Niederer and M. Anliker, Theoretical analysis of arterial hemodynamics including the influence of bifurcations part I, Ann. Biomed. Engrg. 9 (1981) 145-164.

[35] C.A. Taylor, T.J.R. Hughes and C.K. Zarins, Finite element modeling of three–dimensional pulsatile flow in the abdominal aorta: relevance to atherosclerosis, Ann. Biomed. Engrg. 26 (1998) 1–14.

[36] R. Torii, M. Oshima, T. Kobayashi, K. Takagi, T.E. Tezduyar, Computer modeling of cardiovascular fluid-structure interactions with the deforming–spatial–domain/stabilized space-time formulation, Comp. Meth. Appl. Mech. Engrg. 195 (2006) 1885-1895.

[37] S.A. Urquiza, P.J. Blanco, M.J. Vénere and R.A. Feijóo, Multidimensional modelling for the carotid artery blood flow, Comp. Meth. Appl. Mech. Engrg. 195 (2006) 4002–4017.

[38] A. Veneziani, C. Vergara, Flow rate defective boundary conditions in haemodynamics simulations, Int. J. Num. Meth. Fluids 47 (2005) 803–816.

[39] I.E. Vignon–Clementel, C.A. Figueroa, K.E. Jansen and C.A. Taylor, Outflow boundary conditions for three–dimensional finite element modeling of blood flow and pressure in arteries, Comp. Meth. Appl. Mech. Engrg. 195 (2006) 3776–3796.